# Cosmic shear
# 大規模構造による弱い重力レンズ相関関数

浜名崇（国立天文台）

1. 重力レンズの基礎
    1. レンズ方程式、magnification matrix
    2. shearの測定
    3. cosmic shear 2点相関関数 & power spectrum
    4. cosmic shear tomography
2. 銀河のintrinsic alignment、バリオン，ニュートリノの影響
3. 最近の観測結果
4. HSC catalogのlensingに関すること

2016/11/10 ＠国立天文台「秋の学校」

# 重力レンズの基礎ーレンズ方程式

弱場近似のメトリック(c=1)

$$ds^2 = -(1+2\phi)dt^2 + a^2(t)(1-2\phi)(d\chi^2 + f^2(\chi)d\Omega^2)$$

ヌル測地線方程式

$$\frac{d}{d\lambda}k^{\alpha} = -\Gamma^{\alpha}_{\mu\mu}k^{\mu}k^{\nu}$$

これからレンズ方程式が導かれる

（導出は「もうひとつの一般相対論入門」須藤靖）

$$\vec{\theta}(\lambda) = \vec{\theta}_I - 2\int_o^s d\lambda' \frac{D(\lambda-\lambda')}{D(\lambda)}\vec{\nabla}_{\perp}\phi(\lambda')$$

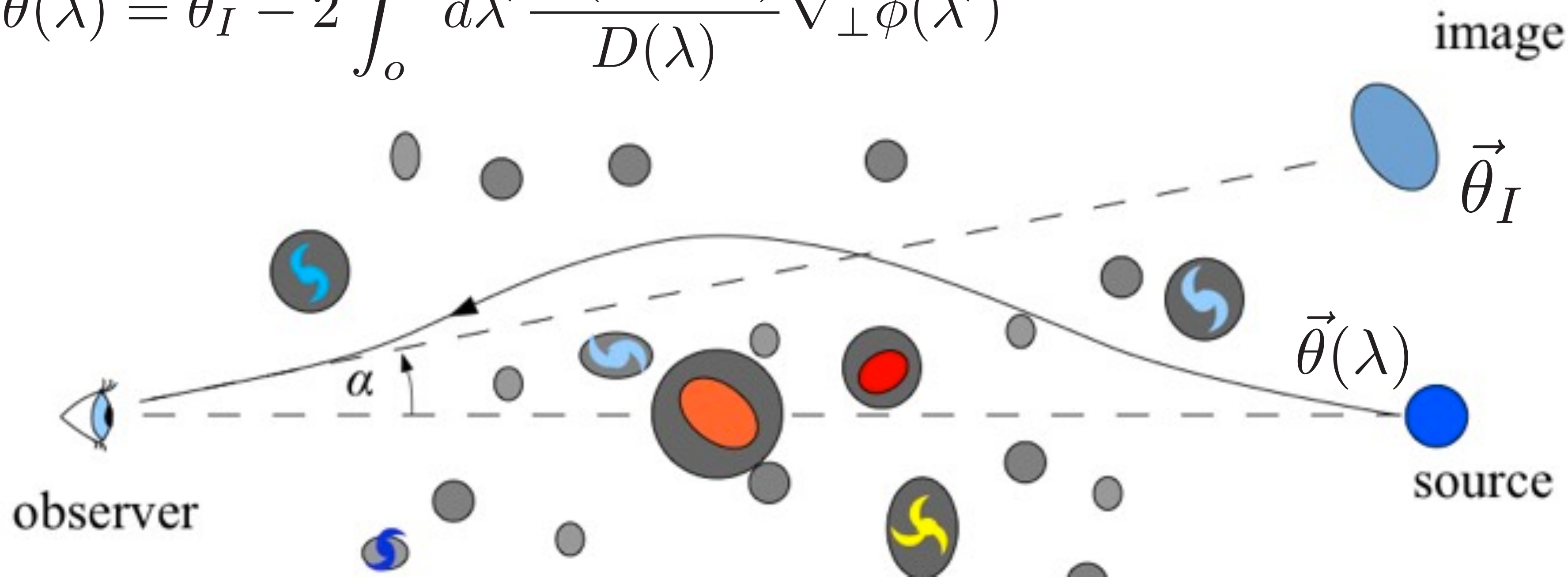

# 重力レンズの基礎ー像の変形(magnification matrix)

微小長離れた光線を結ぶベクトル $Z^\mu$ の測地線偏差方程式

$$\frac{d^2}{d\lambda^2}Z^\mu = -R^\mu_{\alpha\nu\beta}Z^\nu k^\alpha k^\beta$$

光線に垂直な面に射影　$Y^A = e^A_\mu Z^\mu$

$$\frac{d^2}{d\lambda^2}Y_A = \tau_{AB}Y^B$$

さらに $Y^A(\lambda) = M^A{}_B Y^B(\lambda_0)$ として解くと

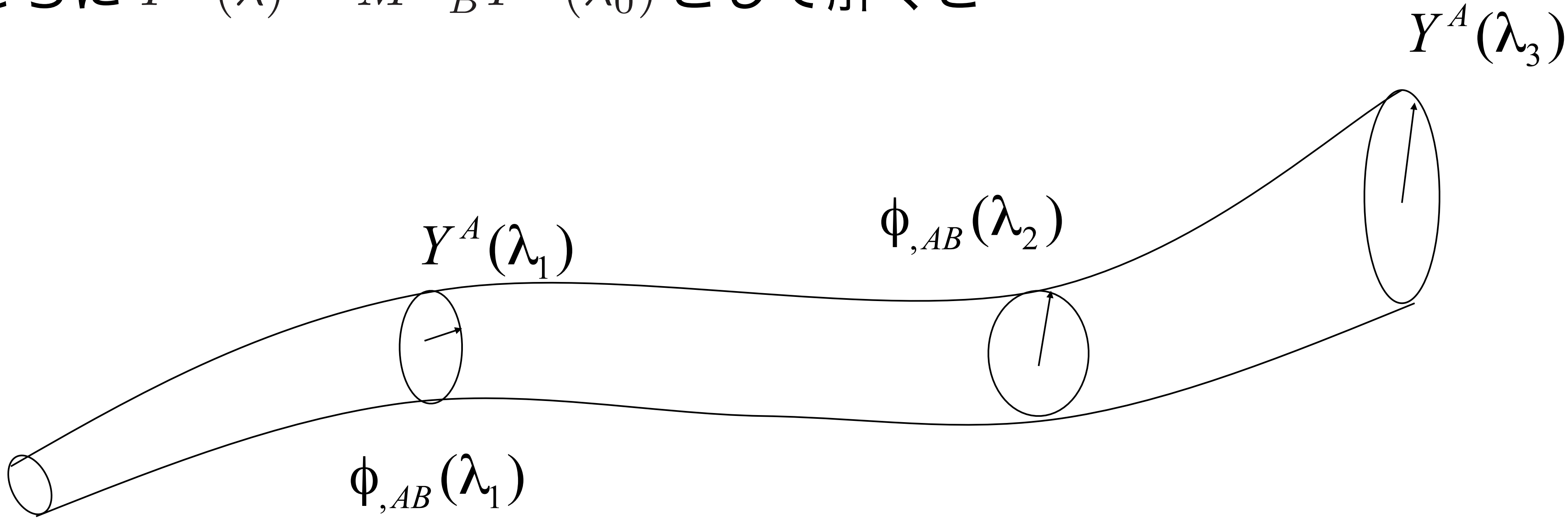

## 重力レンズの基礎ー像の変形 (magnification matrix)

微小長離れた光線を結ぶベクトル $Z^\mu$ の測地線偏差方程式

$$\frac{d^2}{d\lambda^2}Z^\mu = -R^\mu_{\alpha\nu\beta}Z^\nu k^\alpha k^\beta$$

光線に垂直な面に射影　$Y^A = e^A_\mu Z^\mu$

$$\frac{d^2}{d\lambda^2}Y_A = \tau_{AB}Y^B$$

さらに $Y^A(\lambda) = M^A{}_B Y^B(\lambda_0)$ として解くと

$$M_{AB}(\lambda) = \delta_{AB} - \int_o^s d\lambda' \frac{D(\lambda-\lambda')D(\lambda')}{D(\lambda)}\delta\tau_{AC}(\lambda')M_{CB}(\lambda')$$

ここで

$$\delta\tau = \begin{pmatrix} \Delta\phi + (\phi_{,11} - \phi_{,22}) & 2\phi_{,12} \\ 2\phi_{,12} & \Delta\phi - (\phi_{,11} - \phi_{,22}) \end{pmatrix}$$

# 重力レンズの基礎ー像の変形 (magnification matrix)

弱場近似の最低次で

$$M_{AB}(\lambda) \simeq \delta_{AB} - \int_o^s d\lambda' \frac{D(\lambda-\lambda')D(\lambda')}{D(\lambda)} \delta\tau_{AB}(\lambda')$$

これより、convergence, shearと重力場の関係が

以下のように得られる(magnification matrix)

$$M_{AB} = \begin{pmatrix} 1-\kappa-\gamma_1 & -\gamma_2 \\ -\gamma_2 & 1-\kappa+\gamma_2 \end{pmatrix}$$

$$\kappa = 4\pi G \int_o^s d\lambda' \frac{D(\lambda-\lambda')D(\lambda')}{D(\lambda)} \delta\rho(\lambda')$$

$$\gamma_1 = \int_o^s d\lambda' \frac{D(\lambda-\lambda')D(\lambda')}{D(\lambda)} (\phi_{,11}(\lambda') - \phi_{,22}(\lambda'))$$

$$\gamma_2 = \int_o^s d\lambda' \frac{D(\lambda-\lambda')D(\lambda')}{D(\lambda)} 2\phi_{,12}(\lambda')$$

# 重力レンズの基礎ーeffective potential

線形近似の場合２次元potentialを導入すると見通しがよい

$$\psi = 2\int_o^s d\lambda' \frac{D(\lambda-\lambda')D(\lambda')}{D(\lambda)}\phi(\lambda')$$

2次元potentialはconvergenceと２次元Poisson方程式を介して結び付く

$$\psi(\vec{\theta}) = \int d^2\theta' \ln|\vec{\theta}-\vec{\theta'}|\kappa(\vec{\theta'})$$

これを用いるとレンズ方程式は

$$\beta_A = \theta_A(\lambda) = \theta_A - \psi_{,A}$$

magnification matrixはソースとイメージのmappingを表す　$\vec{\theta} = M^{-1}\vec{\beta}$

$$M_{AB}(\lambda) = \frac{\partial\beta_A}{\partial\theta_B} = \delta_{AB} - \psi_{,AB}$$

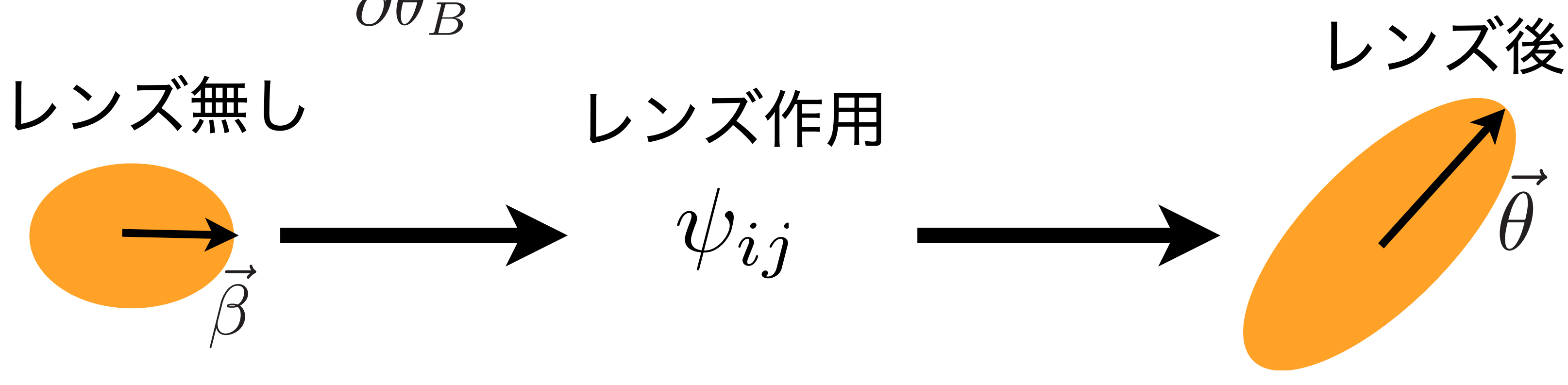

# 重力レンズの基礎ーconvergence & shear

convergenceとshearは

$$
\begin{aligned}
\kappa &= (\psi_{11} + \psi_{22})/2 \\
\gamma_1 &= (\psi_{11} - \psi_{22})/2 \\
\gamma_2 &= \psi_{12}
\end{aligned}
$$

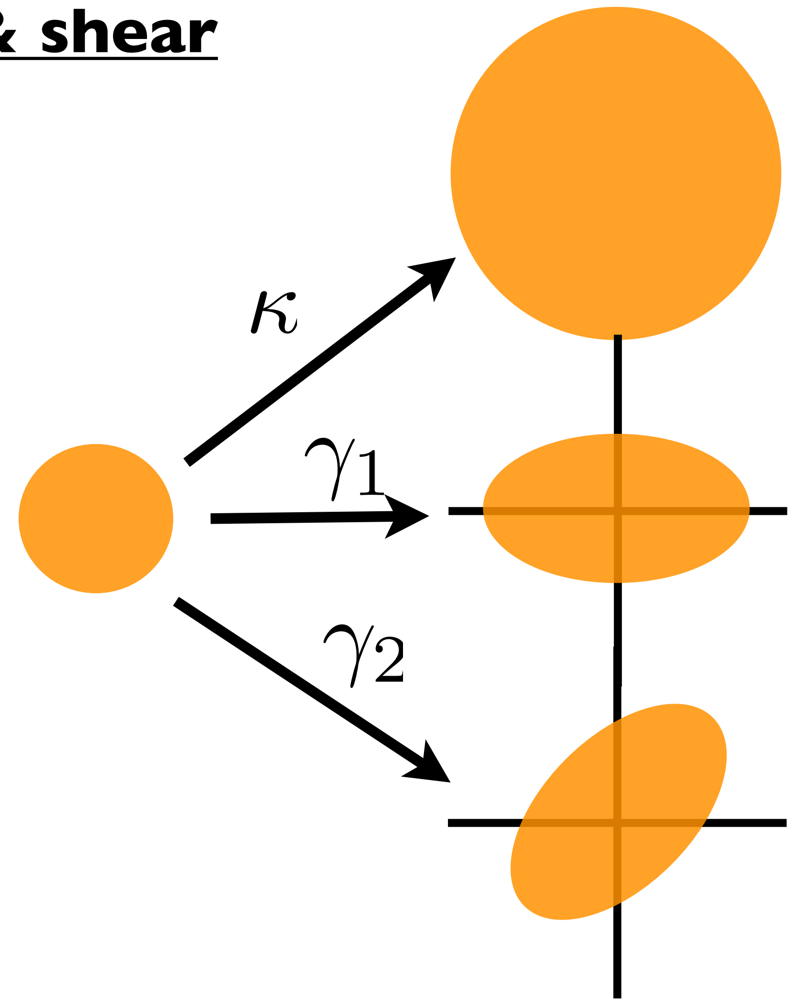


magnification matrixの座標回転は

$$M' = R(\alpha) M R^T(\alpha)$$

これより

$$\kappa' = \kappa$$

$$\begin{pmatrix} \gamma_1' \\ \gamma_2' \end{pmatrix} = \begin{pmatrix} \cos 2\alpha & \sin 2\alpha \\ -\sin 2\alpha & \cos 2\alpha \end{pmatrix} \begin{pmatrix} \gamma_1 \\ \gamma_2 \end{pmatrix}$$

# 重力レンズの基礎ーconvergence & shear

convergenceとshearのフーリエ変換は $\tan\phi_l = \hat{\gamma}_2/\hat{\gamma}_1$

$$\begin{aligned}
\hat{\kappa}(\vec{l}) &= (l_1^2 + l_2^2)\hat{\psi}/2 \\
\hat{\gamma}_1(\vec{l}) &= (l_1^2 - l_2^2)\hat{\psi}/2 = \cos(2\phi_l)\hat{\kappa}(\vec{l}) \\
\hat{\gamma}_2(\vec{l}) &= l_1 l_2 \hat{\psi} = \sin(2\phi_l)\hat{\kappa}(\vec{l})
\end{aligned}$$

これらの関係より、フーリエ空間では（l=0を除いて）$\hat{\gamma} = \hat{\gamma}_1 + i\hat{\gamma}_2$

$$\hat{\kappa} = \frac{l_1^2 - l_2^2 - 2il_1 l_2}{l_1^2 + l_2^2}\hat{\gamma}$$

convergenceとshearは独立な場ではなく、

スカラー重力場の場合shearは自由度１の場

# 重力レンズの基礎ーshearのE/B mode分解

波数ベクトル$(\hat{\gamma}_1, \hat{\gamma}_2)$、の方向 $\phi_l$ への座標回転　$\tan\phi_l = \hat{\gamma}_2/\hat{\gamma}_1$

$$\begin{pmatrix} \hat{\gamma}_E \\ \hat{\gamma}_B \end{pmatrix} = \begin{pmatrix} \cos 2\phi_l & \sin 2\phi_l \\ -\sin 2\phi_l & \cos 2\phi_l \end{pmatrix} \begin{pmatrix} \hat{\gamma}_1 \\ \hat{\gamma}_2 \end{pmatrix}$$

座標に依存しないshearの表現

スカラー重力場では恒等的に $\hat{\gamma}_E = \hat{\kappa}$

$$\hat{\gamma}_B = 0$$

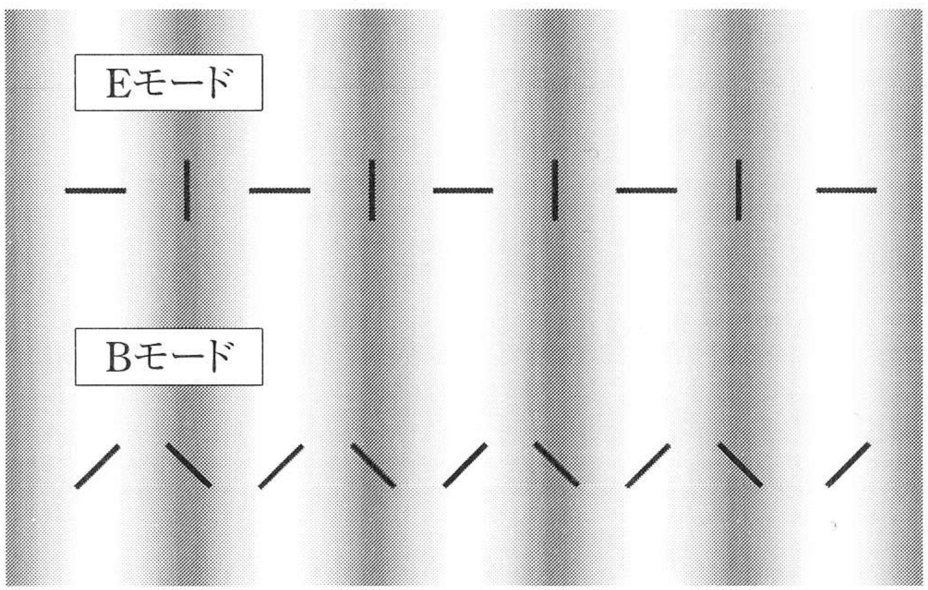


図 9.16　E モードと B モード．ゆらぎの変化する方向に平行あるいは垂直な歪みが E モードであり，斜めを向いた歪みが B モードである．

「現代宇宙論」松原隆彦より

# 重力レンズの基礎ーconvergence & shear power spectrum

＊詳しくは「現代宇宙論」参照

$$\langle\hat{\kappa}(\vec{l})\hat{\kappa}(\vec{l'})\rangle = (2\pi)^2 {\delta_D}^2(\hat{l}+\hat{l}')P_\kappa(l)$$

$$\langle\hat{\gamma}_1(\vec{l})\hat{\gamma}_1(\vec{l'})\rangle = \cos^2(2\phi_l)P_\kappa(l)$$

$$\langle\hat{\gamma}_2(\vec{l})\hat{\gamma}_2(\vec{l'})\rangle = \sin^2(2\phi_l)P_\kappa(l)$$

→ $P_{\gamma_1}(l) + P_{\gamma_2}(l) = P_\kappa(l)$

E/B mode分解したshearに対しても同様に定義されて

$$P_{\gamma_E}(l) + P_{\gamma_B}(l) = P_{\gamma_1}(l) + P_{\gamma_2}(l)$$

スカラー重力potentialの場合

$$P_{\gamma_E}(l) = P_\kappa(l)$$

$$P_{\gamma_B}(l) = 0$$

# 重力レンズの基礎ーconvergence & shear ２点相関関数

＊詳しくは「現代宇宙論」参照

$$\xi_\kappa(\theta_{12}) = \langle \kappa(\vec{\theta_1})\kappa(\vec{\theta_2})\rangle$$

２点相関関数はpower spectrumのフーリエ変換なので

$$\xi_\kappa(\theta_{12}) = \xi_{\gamma_E}(\theta_{12}) = \frac{1}{2\pi}\int dl\ lP_\kappa(l)J_0(l\theta)$$

２つの天体を結ぶ線を１軸とした座標系でshearを定義した場合

$$\begin{pmatrix} \gamma_t \\ \gamma_\times \end{pmatrix} = \begin{pmatrix} \cos 2\alpha & \sin 2\alpha \\ -\sin 2\alpha & \cos 2\alpha \end{pmatrix} \begin{pmatrix} \gamma_1 \\ \gamma_2 \end{pmatrix}$$

$$\begin{aligned} \xi_+(\theta_{12}) &= \xi_{tt}(\theta_{12}) + \xi_{\times\times}(\theta_{12}) \\ &= \frac{1}{2\pi}\int dl\ lP_\kappa(l)J_0(l\theta) \end{aligned}$$

$$\begin{aligned} \xi_-(\theta_{12}) &= \xi_{tt}(\theta_{12}) - \xi_{\times\times}(\theta_{12}) \\ &= \frac{1}{2\pi}\int dl\ lP_\kappa(l)J_4(l\theta) \end{aligned}$$

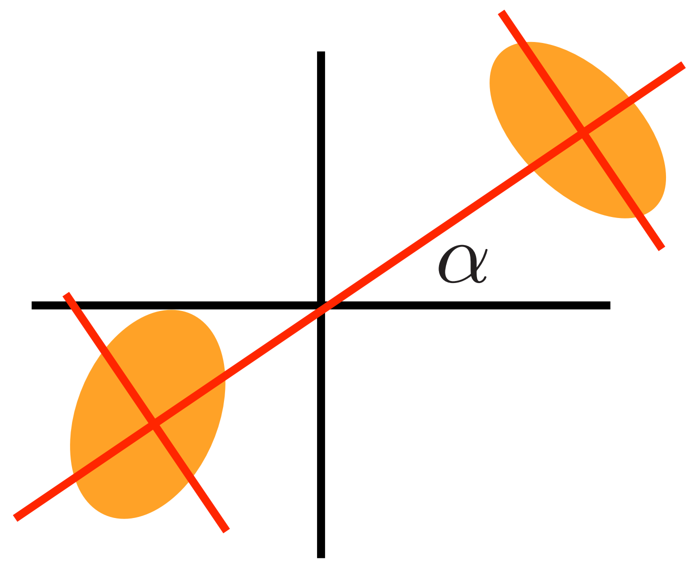

# shearの測定

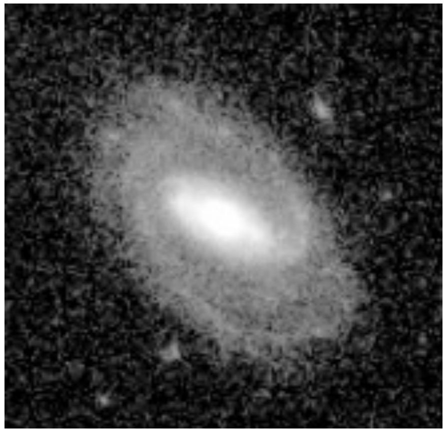

$$Q_{ij} = \int d\theta^2 \theta_i \theta_j W(\theta) f(\theta)$$

$$e_1 = \frac{Q_{11} - Q_{22}}{Q_{11} + Q_{22}}$$

$$e_2 = \frac{2Q_{12}}{Q_{11} + Q_{22}}$$

$$e = e_1 + ie_2$$

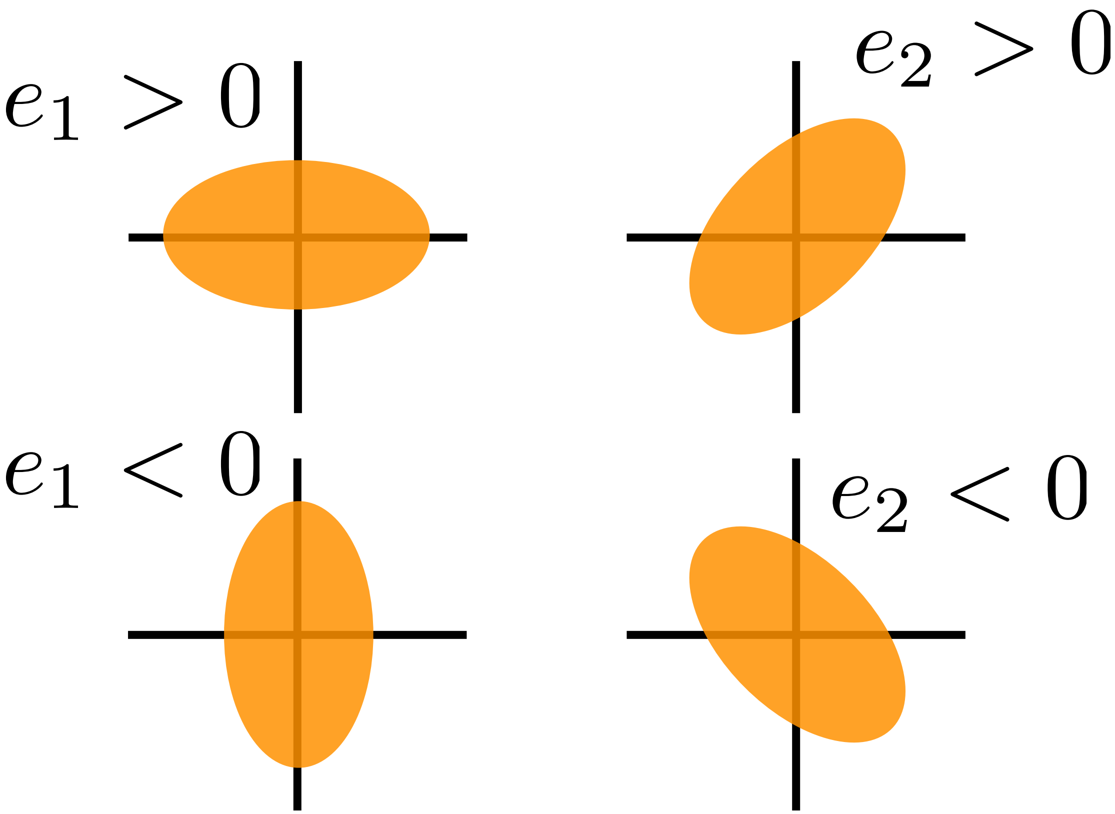


for a uniform ellipse

$$e = \frac{1 - (b/a)^2}{1 + (b/a)^2}$$

$$\left( e = \sqrt{e_1^2 + e_2^2} \right)$$

$$\frac{b}{a} \sim 1 - e$$

**shearの測定**　＊ここではPSFの影響は除外している

レンズ効果を受ける前の輝度分布２次モーメントテンソルを $Q^s$

とすると観測された $Q$ との関係はmagnification matrixによる作用から

$Q^S = MQM^T = MQM$　　また　$Q = M^{-1}Q^s M^{-1}$

後者を具体的に書き下して整理すると、（ただし $g = \gamma/(1-\kappa)$ ）

$$e = \frac{e^s + 2g + g^2 e^{s*}}{1 + |g|^2 + 2\mathrm{Re}(g e^{s*})}$$

gについて線形近似をとると

$$e = e^s + 2g - 2e^s \mathrm{Re}(g e^{s*})$$

とある領域中で $e^s$ には空間相間がないとして平均をとると

$$\langle e \rangle \simeq 2g - g\langle e^{s2} \rangle \rightarrow \quad g \simeq \gamma \simeq \frac{\langle e \rangle}{2(1-\sigma_{e^s}^2)} \qquad \sigma_{e^s}^2 = \langle e_1^{s2} + e_2^{s2} \rangle / 2$$

ここで $\sigma_{e^s}$ は1成分RMSで観測可能な $\sigma_e$ で代用する

＊詳しくは「現代宇宙論」「ワインバーグの宇宙論」参照

# shearの測定

photon統計noiseや不完全なPSF補正により、計測されたshearはバイアスされている、一般に以下のようにモデル化する

$$\gamma_{obs} = (1+m)\gamma_{true} + c$$

•一般に、 $(m, c)$ は数パーセントのオーダー

•$(m, c)$は、image simulationを用いて評価する。一般に銀河のfluxとsizeの関数として表現される。

✴HSC surveyの場合、現在image simulationを実施中。

$(m, c)$をfluxとsizeの関数としてfitしたものを公開する予定。

# shear2点相間関数の測定

shearのestimator $\tilde{\gamma}$ とその計測誤差から定義した重みwから

$$\xi_{\pm}(\theta_{i\text{-bin}}) = \frac{\sum w_A w_B (\tilde{\gamma}_t(\theta_A)\tilde{\gamma}_t(\theta_B) \pm \tilde{\gamma}_\times(\theta_A)\tilde{\gamma}_\times(\theta_B))}{\sum w_A w_B}$$

統計誤差は(詳しくは Schneider et al 2002, A&A, 396, 1)

$$Var\left[\xi_{\pm}(\theta_{i\text{-bin}})\right] = \frac{(\sigma^2_{\tilde{\gamma}_t} + \sigma^2_{\tilde{\gamma}_\times})^2}{N_{pair}(\theta_{i\text{-bin}})}$$

Cosmic varianceは

(詳しくは Sato et al 2011, ApJ, 734, 76)

$$\mathrm{Cov}[\xi_+(\theta), \xi_+(\theta')] = \frac{1}{\pi\Omega_s}\int_0^\infty l dl\, J_0(l\theta) J_0(l\theta') P_\kappa(l)^2 + \frac{1}{4\pi^2\Omega_s}\int_0^\infty l dl \int_0^\infty l' dl'\, J_0(l\theta) J_0(l'\theta') \bar{T}_\kappa(l, l'),$$

A=25sq deg

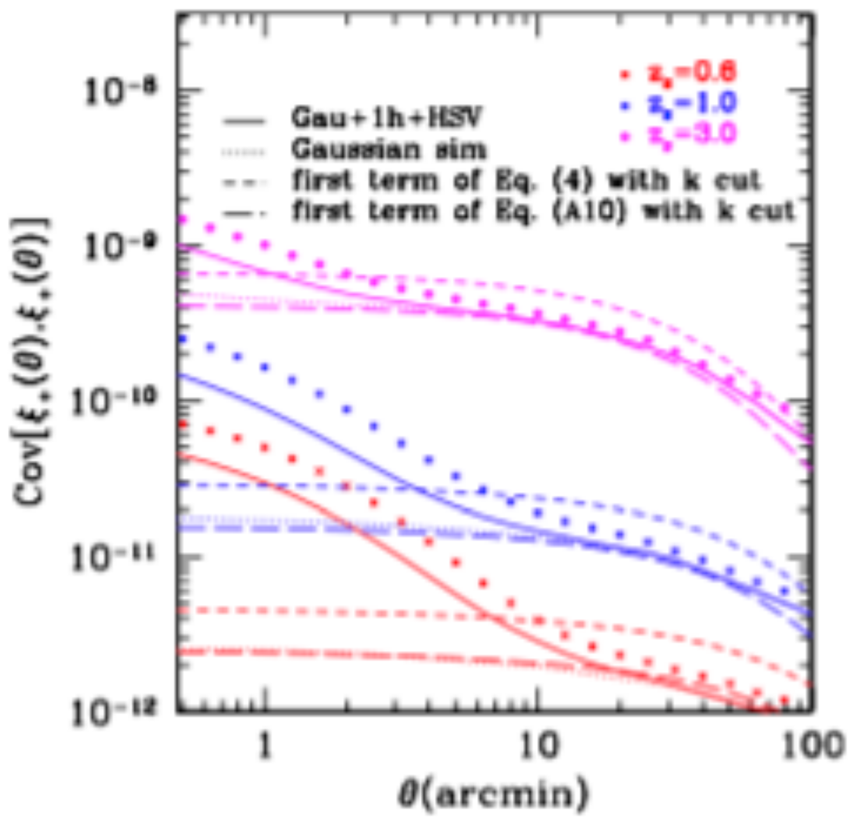

# shear power spectrumの測定

Pseudo-power-spectrum method (Hikage et al, 2011, MNRAS, 412, 65)
理想的には

$$E_{lm} \pm \mathrm{i}B_{lm} = \oint \mathrm{d}\Omega_{\hat{\boldsymbol{n}}} \, [\gamma_1(\hat{\boldsymbol{n}}) \pm \mathrm{i}\gamma_2(\hat{\boldsymbol{n}})] \; {}_{\pm 2}Y^*_{lm}(\hat{\boldsymbol{n}}),$$

$$C_l^{EE} \equiv \frac{1}{2l+1}\sum_m |E_{lm}|^2, \qquad C_l^{BB} \equiv \frac{1}{2l+1}\sum_m |B_{lm}|^2,$$

実際にはsurvey領域や、明るい星などによるデータ欠落領域があり

$$\tilde{E}_{lm} \pm \mathrm{i}\tilde{B}_{lm} = \oint \mathrm{d}\Omega_{\hat{\boldsymbol{n}}} \, [K(\hat{\boldsymbol{n}})(\gamma_1(\hat{\boldsymbol{n}}) \pm \mathrm{i}\gamma_2(\hat{\boldsymbol{n}}))] \, {}_{\pm 2}Y^*_{lm}(\hat{\boldsymbol{n}}).$$

これは真のshear場と

$$\tilde{E}_{lm} \pm \mathrm{i}\tilde{B}_{lm} = \sum_{l'm'} (E_{l'm'} \pm \mathrm{i}B_{l'm'})_{\pm 2}W_{ll'mm'},$$

$$\begin{aligned}
{}_{\pm 2}W_{ll'mm'} &\equiv \oint \mathrm{d}\Omega_{\hat{\boldsymbol{n}}\,\pm 2}Y_{l'm'}(\hat{\boldsymbol{n}})K(\hat{\boldsymbol{n}})_{\pm 2}Y^*_{lm}(\hat{\boldsymbol{n}}) \\
&= \sum_{l''m''} K_{l''m''}(-1)^m \sqrt{\frac{(2l+1)(2l'+1)(2l''+1)}{4\pi}} \\
&\quad \times \begin{pmatrix} l & l' & l'' \\ \pm 2 & \mp 2 & 0 \end{pmatrix} \begin{pmatrix} l & l' & l'' \\ m & m' & m'' \end{pmatrix},
\end{aligned}$$

$$K_{lm} = \oint \mathrm{d}\Omega_{\hat{\boldsymbol{n}}} K(\hat{\boldsymbol{n}}) Y^*_{lm}(\hat{\boldsymbol{n}}).$$

# shear power spectrumの測定

統計誤差は(詳しくは Joachimi et al 2008, A&A, 477, 43)

$$Var\left[P_{\gamma_E}(l)\right] = \frac{(\sigma^2_{\tilde{\gamma}_t} + \sigma^2_{\tilde{\gamma}_\times})^2}{4n_g}$$

Cosmic varianceは (詳しくは Sato et al 2009, ApJ, 701, 945)

$$\begin{aligned}\mathrm{Cov}[P_\kappa(l), P_\kappa(l')] &\equiv \langle(\hat{P}_\kappa(l) - P_\kappa(l))(\hat{P}_\kappa(l') - P_\kappa(l'))\rangle \\ &= \frac{2}{N_l} P_\kappa(l)^2 \delta^K_{l,l'} \\ &+ \frac{1}{\Omega_s}\int_l \frac{d^2\boldsymbol{l}}{A_s}\int_{l'} \frac{d^2\boldsymbol{l}'}{A_{s'}} T(\boldsymbol{l}, -\boldsymbol{l}, \boldsymbol{l}', -\boldsymbol{l}'),\end{aligned}$$

A=25sq deg

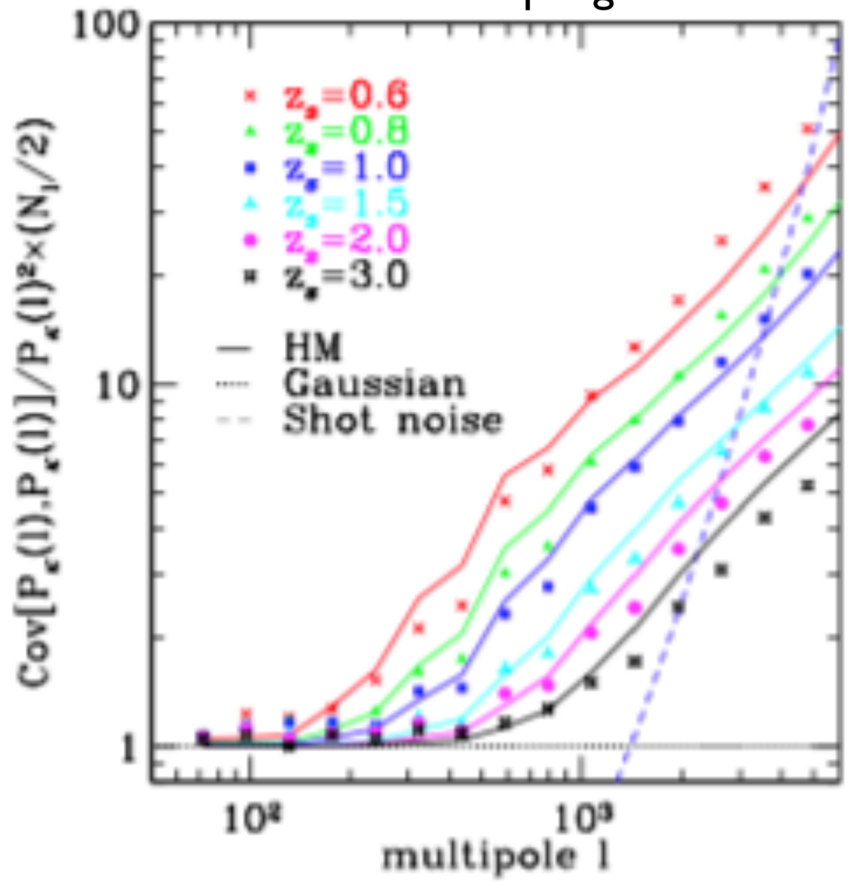

# 重力レンズの基礎ーcosmic shear power spectrum 理論モデル

＊詳しくは「現代宇宙論」参照

$$P_\kappa(l) = \frac{9H_0^4\Omega_m^2}{4c^4}\int_0^\infty d\chi \frac{g^2(\chi)}{a^2(t)D^2(\chi)} P_m\left[\frac{l}{D(\chi)}, t\right]$$

$$\xi_\kappa(\theta) = \frac{9H_0^4\Omega_m^2}{4c^4}\int_0^\infty d\chi \frac{g^2(\chi)}{a^2(t)} \int \frac{dkk}{2\pi} J_0(kD(\chi)\theta) P_m(k,t)$$

ここで、lensing efficiency function

$$g(\chi_l) = D(\chi_l)\int_{\chi_l}^\infty d\chi_s \; n_s(\chi_s)\frac{D(\chi_s - \chi_l)}{D(\chi_s)}$$

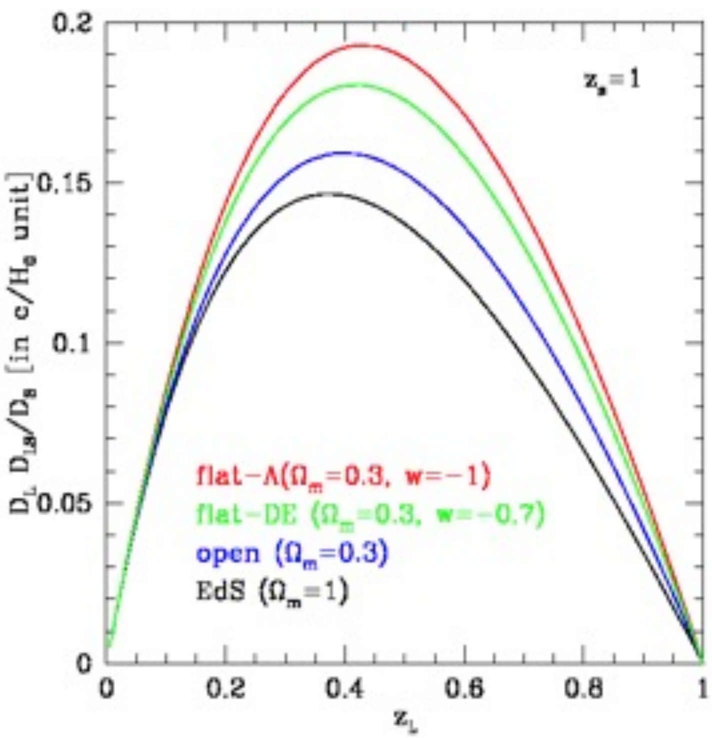


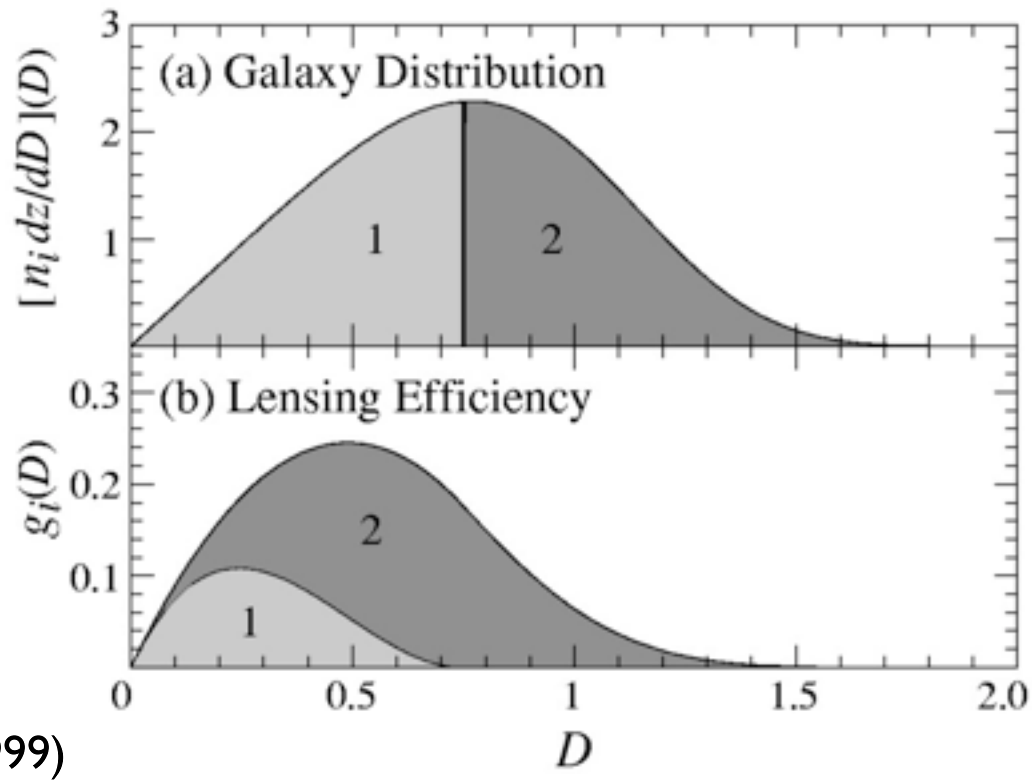


Hu (1999)

# 重力レンズの基礎ーcosmic shear tomography

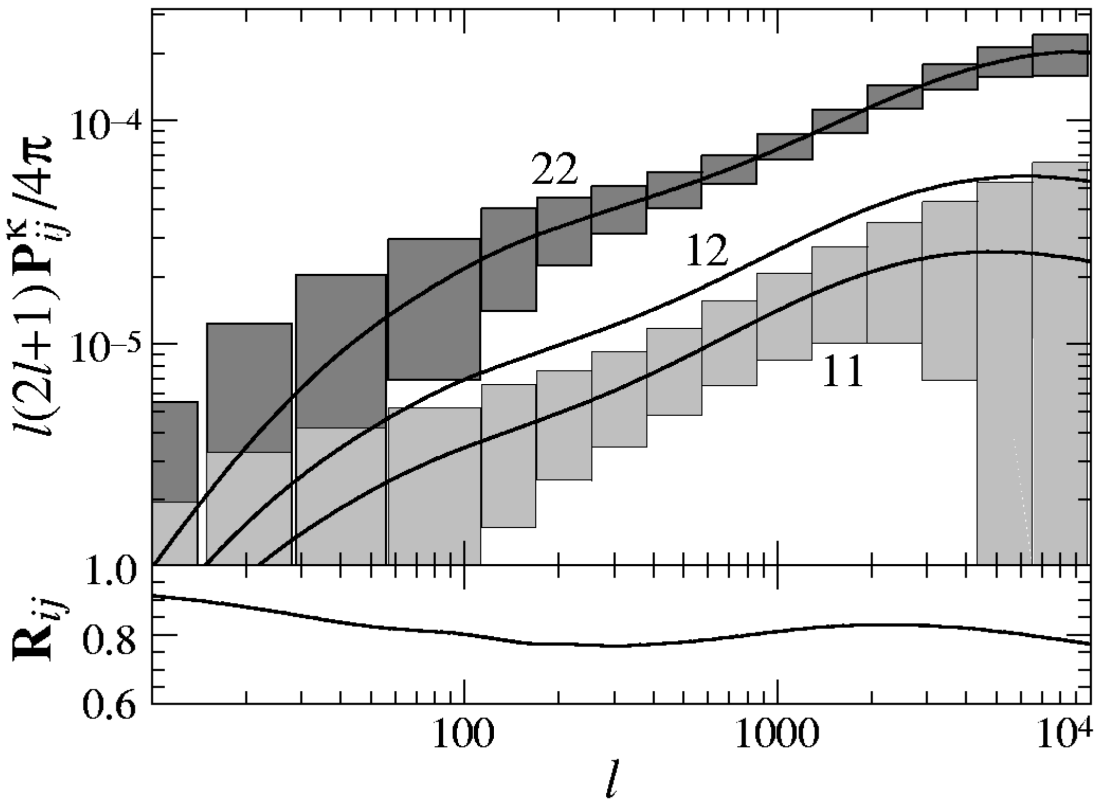


FIG. 2.—Power spectra and cross-correlation for a subdivision in two across the median redshift $z_{\rm median} = 1$ and errors for a survey of 5° on the side, $\langle \gamma^2_{\rm int} \rangle^{1/2} = 0.4$, and $\bar{n} = 2 \times 10^5$ deg$^{-2}$. Note the strong correlation $\boldsymbol{R}_{ij}$ between the two power spectra make the combination of the power spectra less constraining than a naive interpretation of the individual errors would imply.

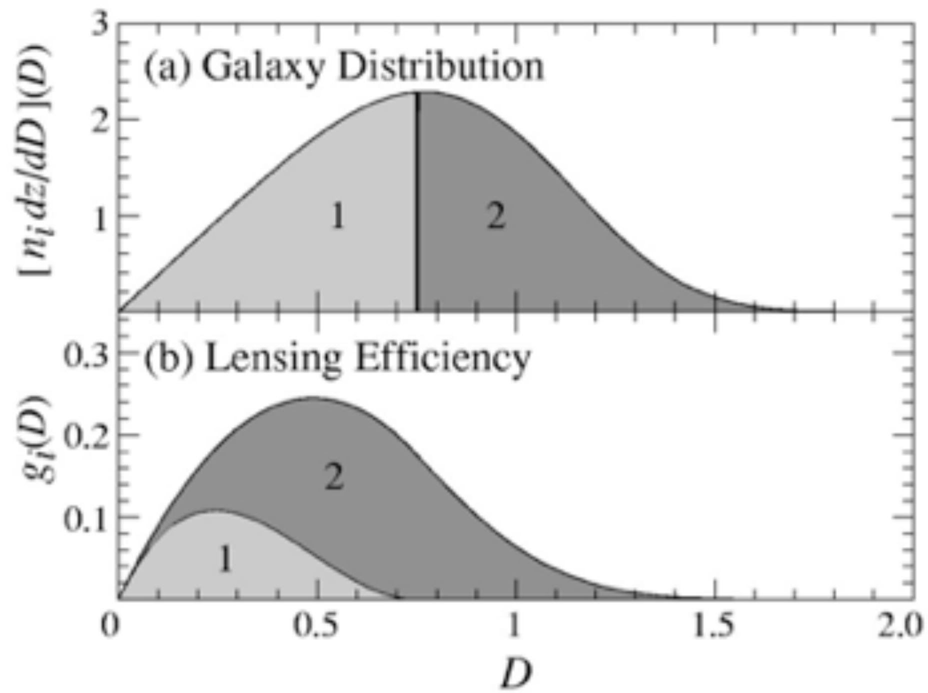


Hu (1999)

# 重力レンズの基礎ーcosmic shear tomography

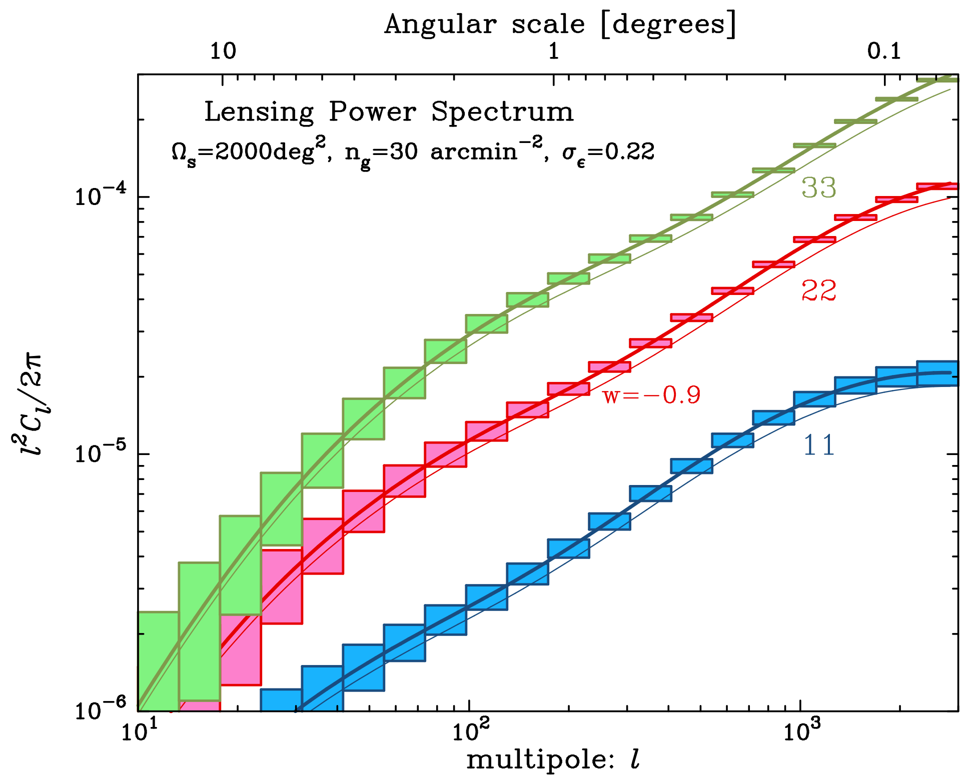


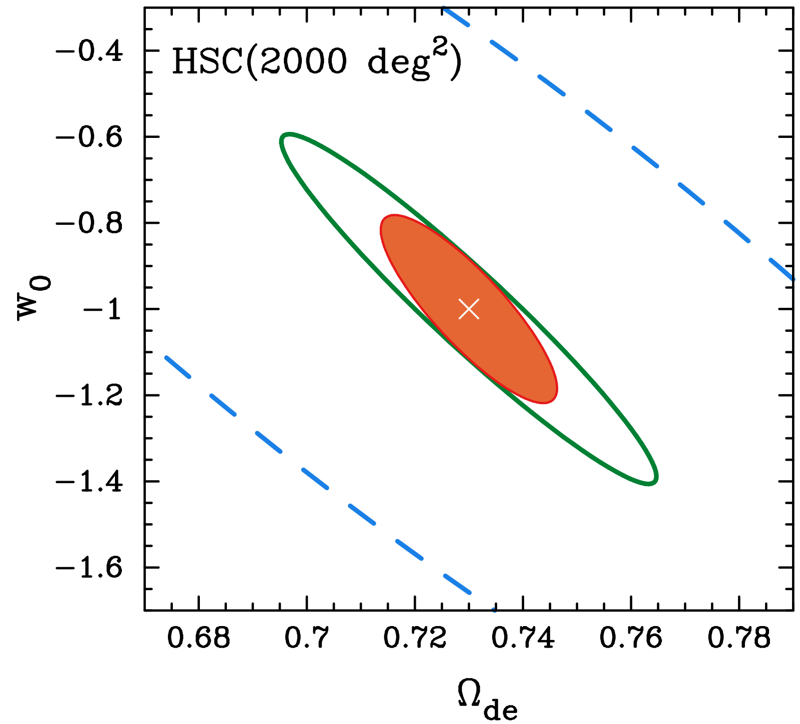


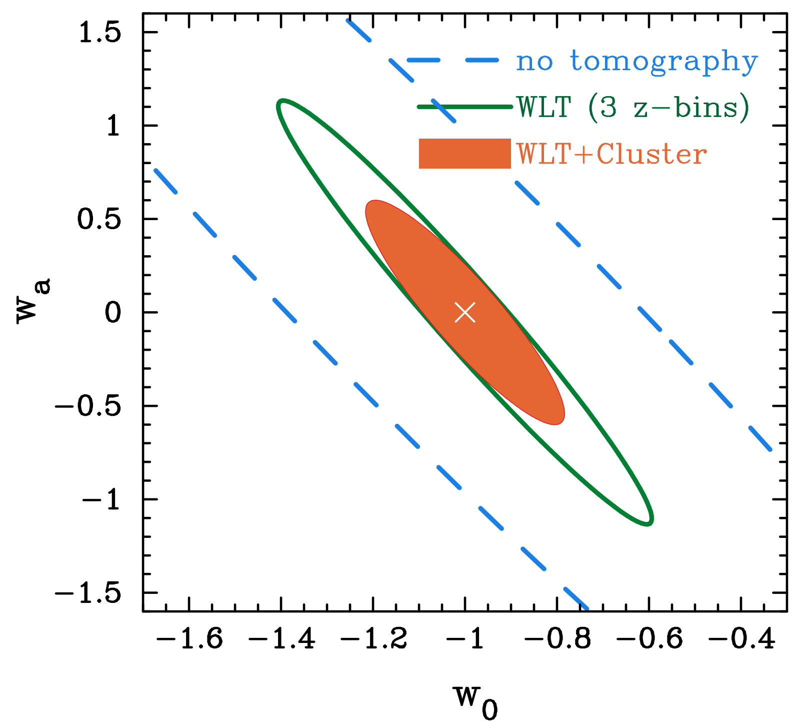


$$0 \leq z_1 \leq 0.6,\ 0.6 \leq z_2 \leq 1, \text{ and } z_3 \geq 1.$$

HSC survey White paper

# ソース銀河のredshift分布の推定

(1) photometric redshiftとは

flux(g,r,i,z,y,+)とmodel SEDのfitting

→PDF(zp)

→point estimate(median, mean,mode)
　その信憑性（PDFの広がりなど）

(2) point estimateとその信憑性からあるredshift binに入る銀河を選択

(3) 選択された銀河のPDF(zp)を足し合わせて、真（？）のredshift分布を推測

(4) 分光redshiftがある銀河のPDF(zp)を用いて(3)のPDF(zp)を矯正

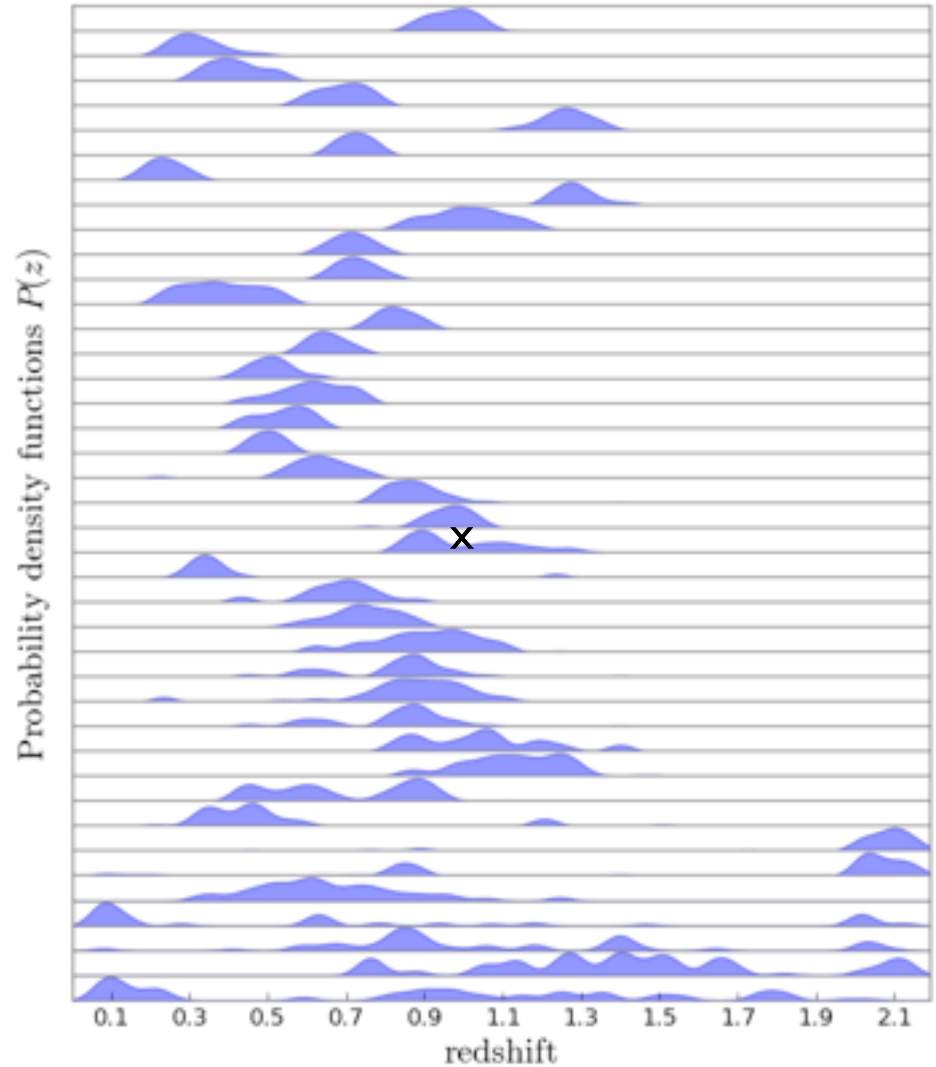

# ソース銀河のredshift分布の推定

KiDS survey (Hildebrandt et al 2016 arXiv:1606:05338)

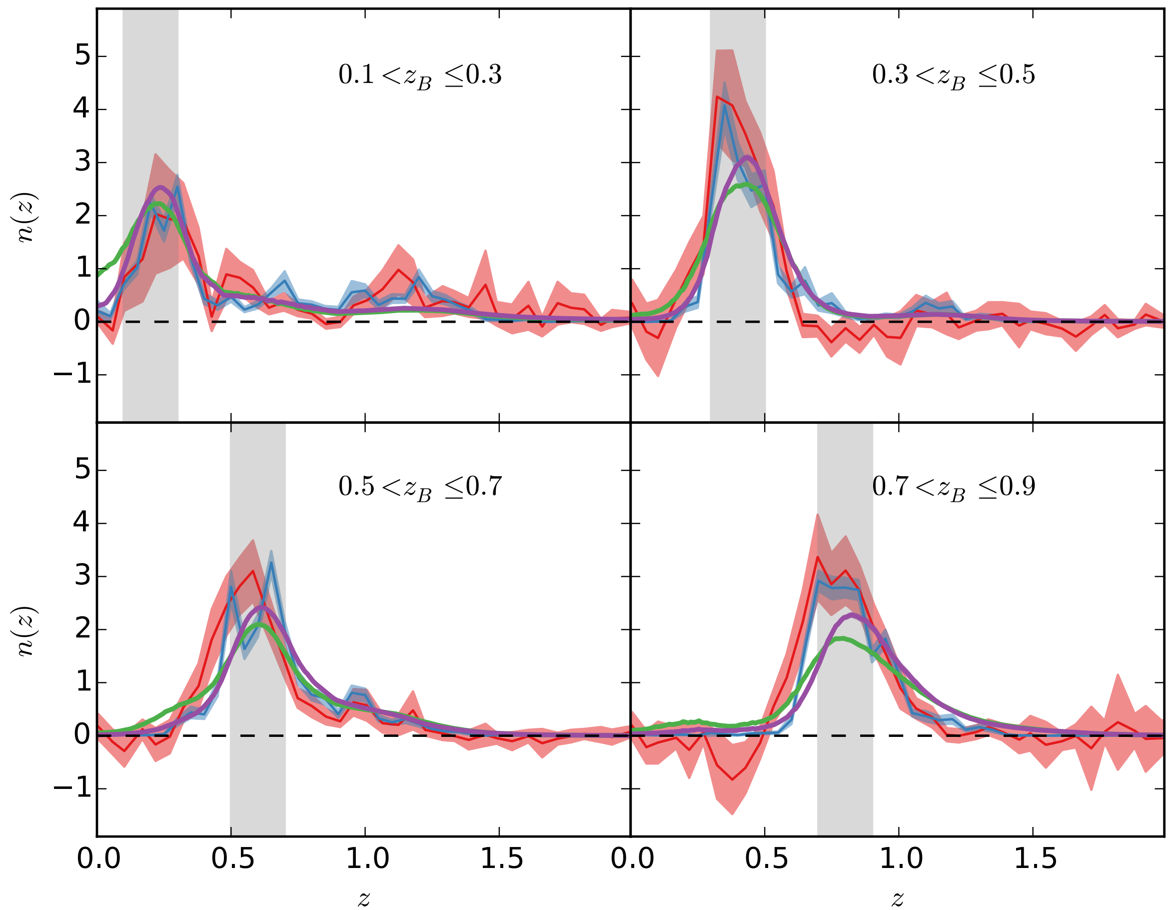


**Figure 2.** Comparison of the normalised redshift distributions for the four tomographic bins as estimated from the weighted direct calibration (DIR, blue with errors), the calibration with cross-correlations (CC, red with errors), the re-calibrated stacked $P_{\rm recal}(z)$ (BOR, purple with errors that are barely visible), and the original stacked $P(z)$ from BPZ (green). The gray-shaded regions indicate the target redshift range selected by cuts on the Bayesian photo-$z$ $z_{\rm B}$. Errors shown here do not include the effects of sample variance in the spec-$z$ calibration sample.

$$g(\chi_l) = D(\chi_l)\int_{\chi_l}^{\infty} d\chi_s\, n_s(\chi_s)\frac{D(\chi_s-\chi_l)}{D(\chi_s)}$$

$$P_\kappa(l) = \frac{9H_0^4\Omega_m^2}{4c^4}\int_0^{\infty} d\chi \frac{g^2(\chi)}{a^2(t)D^2(\chi)} P_m\left[\frac{l}{D(\chi)}, t\right]$$

# 銀河のintrinsic alignmentの影響

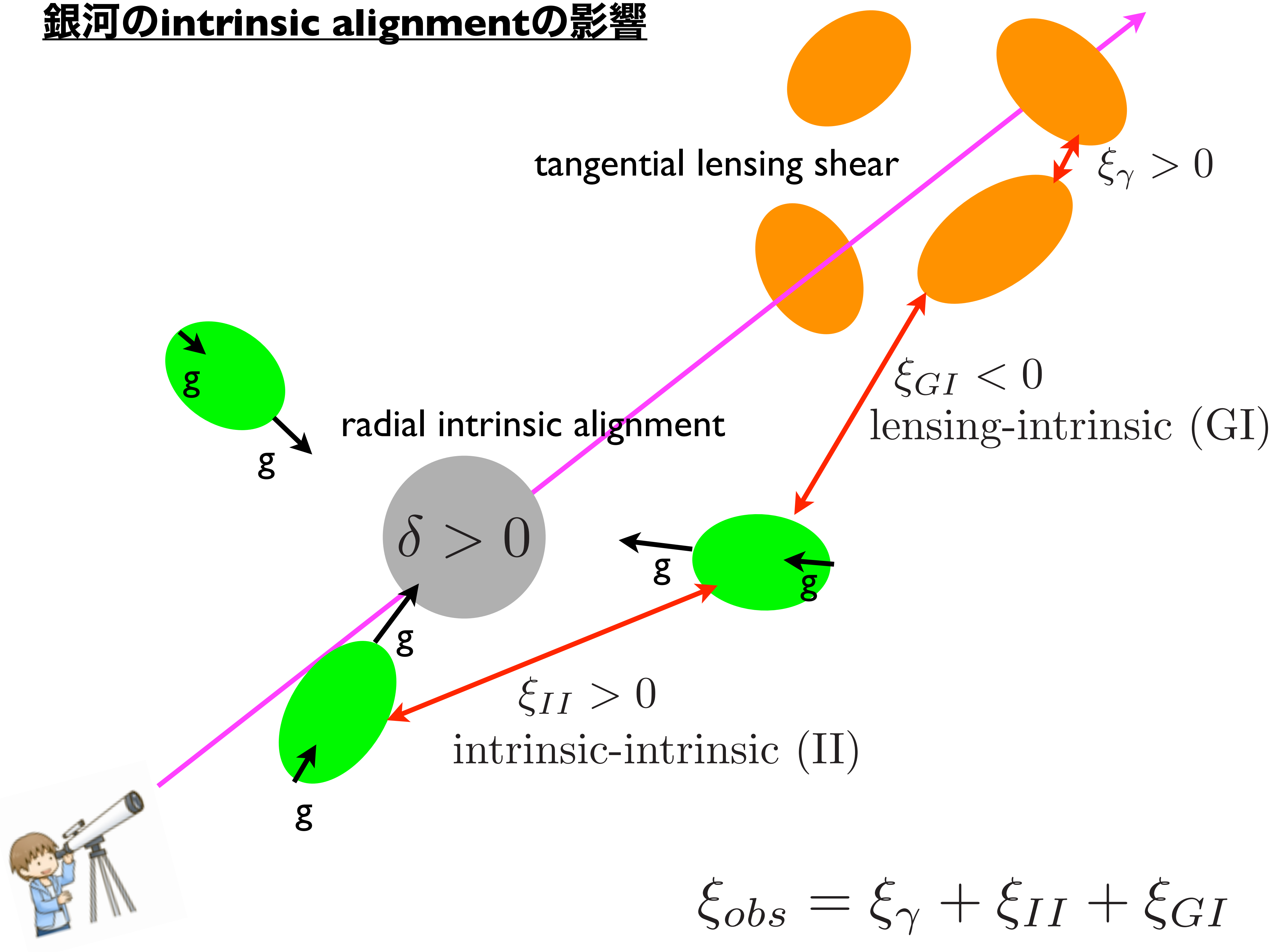


$$\xi_{obs} = \xi_\gamma + \xi_{II} + \xi_{GI}$$

# 銀河のintrinsic alignmentの観測

Joachimi et al 2011

Okumura & Jing 2009

SDSS LRG

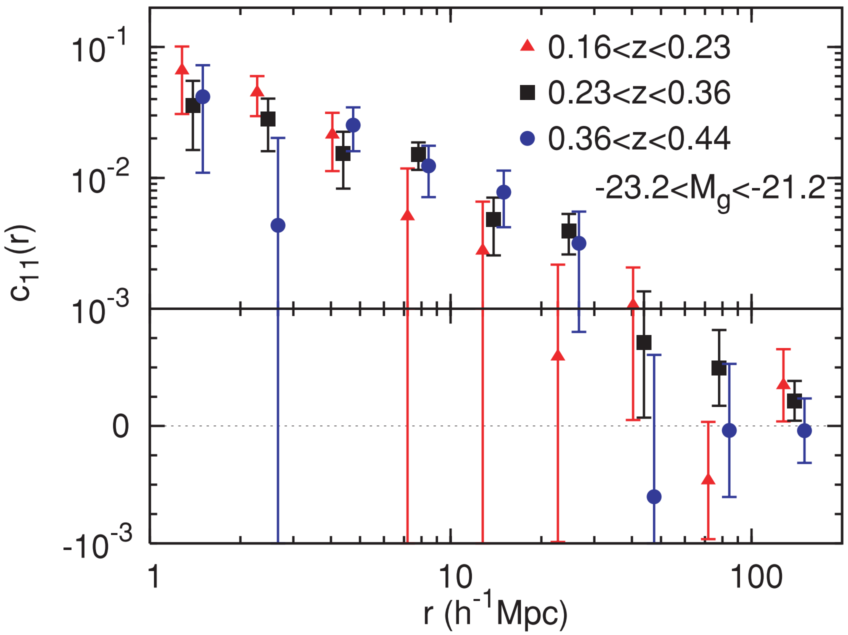


**Figure 4.** Redshift dependence of $c_{11}(r)$ of the LRGs for the absolute magnitude of $-23.2 < M_g < -21.2$. Here both the central and satellite LRGs are used for the calculation. Note that the vertical axis mixes logarithmic and linear scalings.

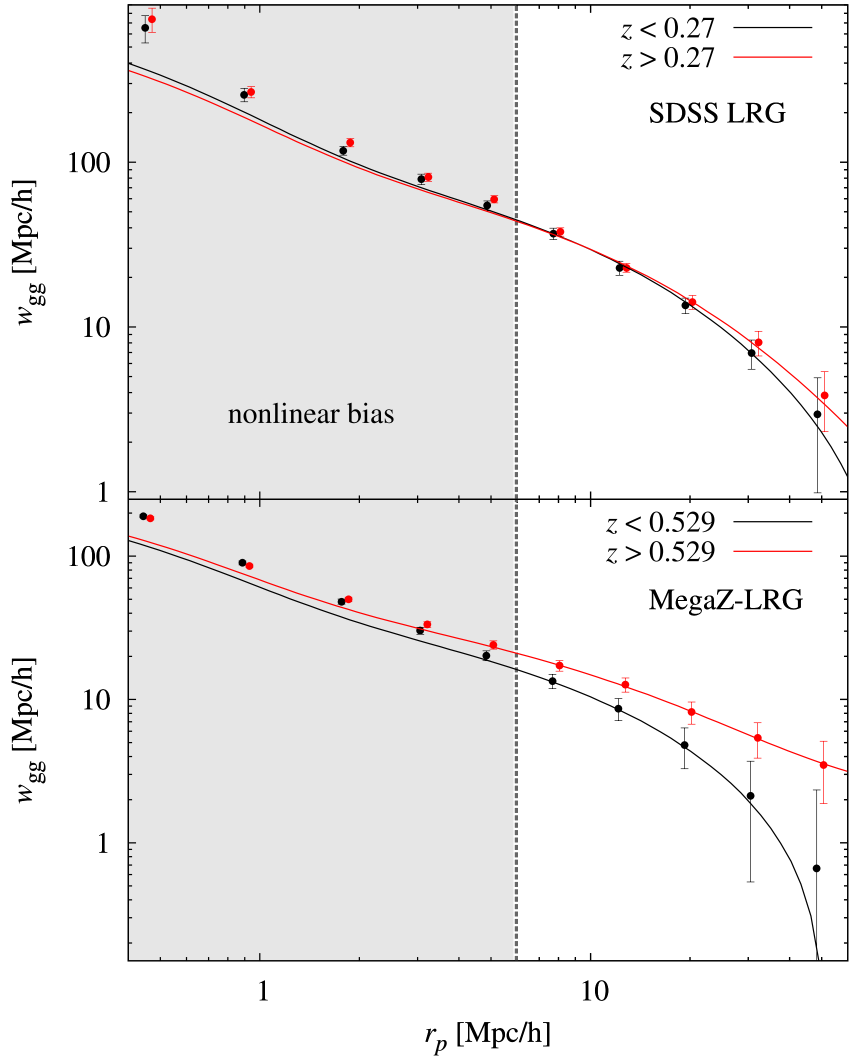


**Fig. 8.** Projected correlation function $w_{gg}$ as a function of comoving transverse separation $r_p$. *Top panel*: for the SDSS LRG sample with redshifts smaller than 0.27 (black) and with redshifts larger than 0.27 (red). *Bottom panel*: for the MegaZ-LRG sample with photometric redshifts smaller than 0.529 (black) and with photometric redshifts larger than 0.529 (red). Note that the red points have been slightly offset horizontally for clarity, and that the error bars are strongly correlated. In addition we show the best-fit models as black and red curves, respectively. Only the data points outside the grey region have been used for the fits to avoid the regime of nonlinear bias.

## 銀河のintrinsic alignmentの理論モデル

Intrinsic alignmentの主要因が潮汐力だとすると、それによる変形はlensingの場合と同様にpotentialの微分で書けるはずで

$$e_{IA} \propto (\phi_{,11} - \phi_{,22}, 2\phi_{,12})$$

これからprojected ellipticity correlationは、lensing shearの場合と同様にして、matter power spectrumで書けて

$$\begin{aligned} P_{\mathrm{II}}(k,z) &= F^2(z) P_\delta(k,z) \\ P_{\mathrm{GI}}(k,z) &= F(z) P_\delta(k,z)\,, \end{aligned} \tag{7}$$

潮汐力とeとの関係やそのredshiftやluminosity関係はパラメータを導入して

$$F(z) = -A_{\mathrm{IA}} C_1 \rho_{\mathrm{crit}} \frac{\Omega_{\mathrm{m}}}{D_+(z)} \left(\frac{1+z}{1+z_0}\right)^\eta \left(\frac{\bar{L}}{L_0}\right)^\beta . \tag{8}$$

# Matter power spectrumへのバリオンの影響

•small scaleではbaryon physics（gas-cooling, supernova feedback, AGN feedback）がtotal matter power spectrumに影響を及ぼす

•baryon physicsの詳細については不明な点が多いが、hydro simulationの結果をもとにmatter power spectrumにfree parameter "B"を導入

•KiDS論文では、2<B<4、この範囲はOWLS simulationから予想される範囲で、下図(Mead+2015)のspread程度

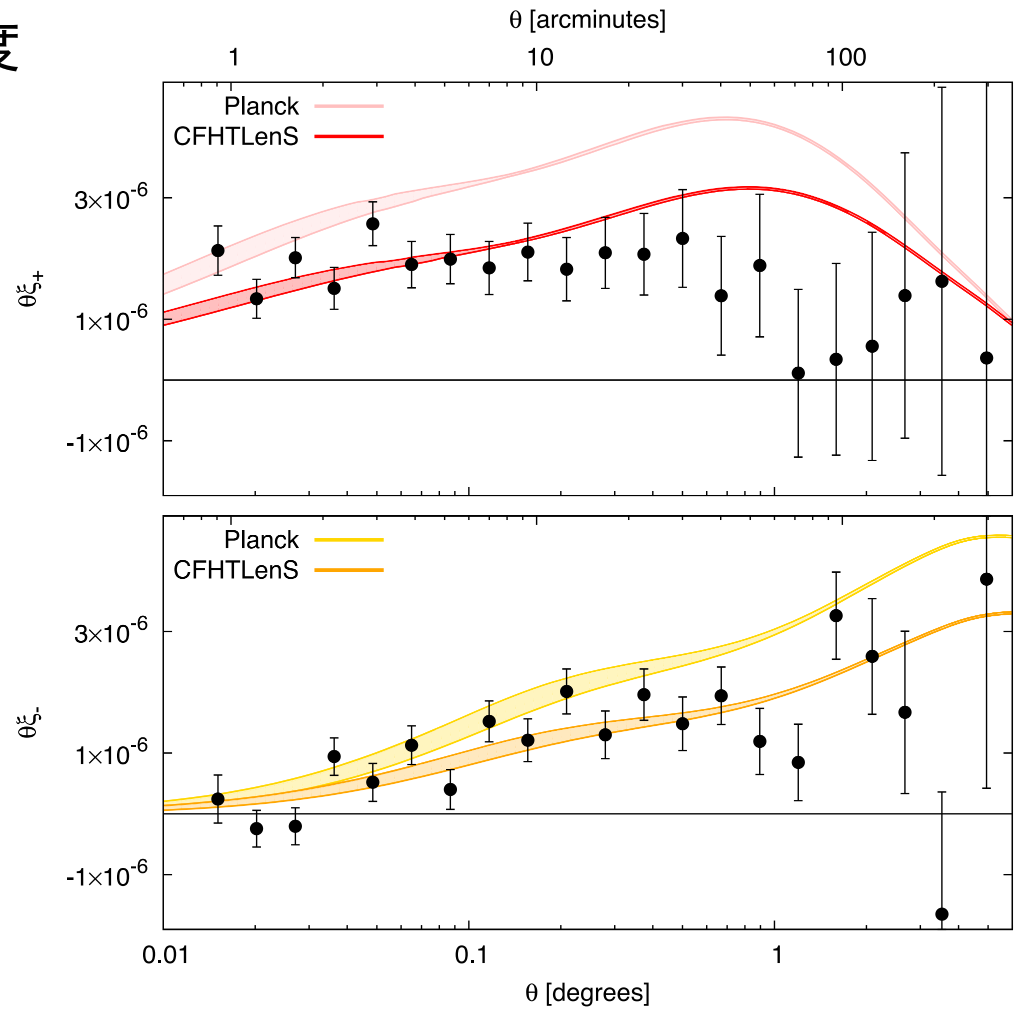

# Matter power spectrumへのニュートリノの影響

- 詳しくは昨日の市来氏の講演を参照
- ニュートリノのfree-streamingによるsmall scale (<100Mpc)の構造形成が遅れる

Ichiki et al 2009

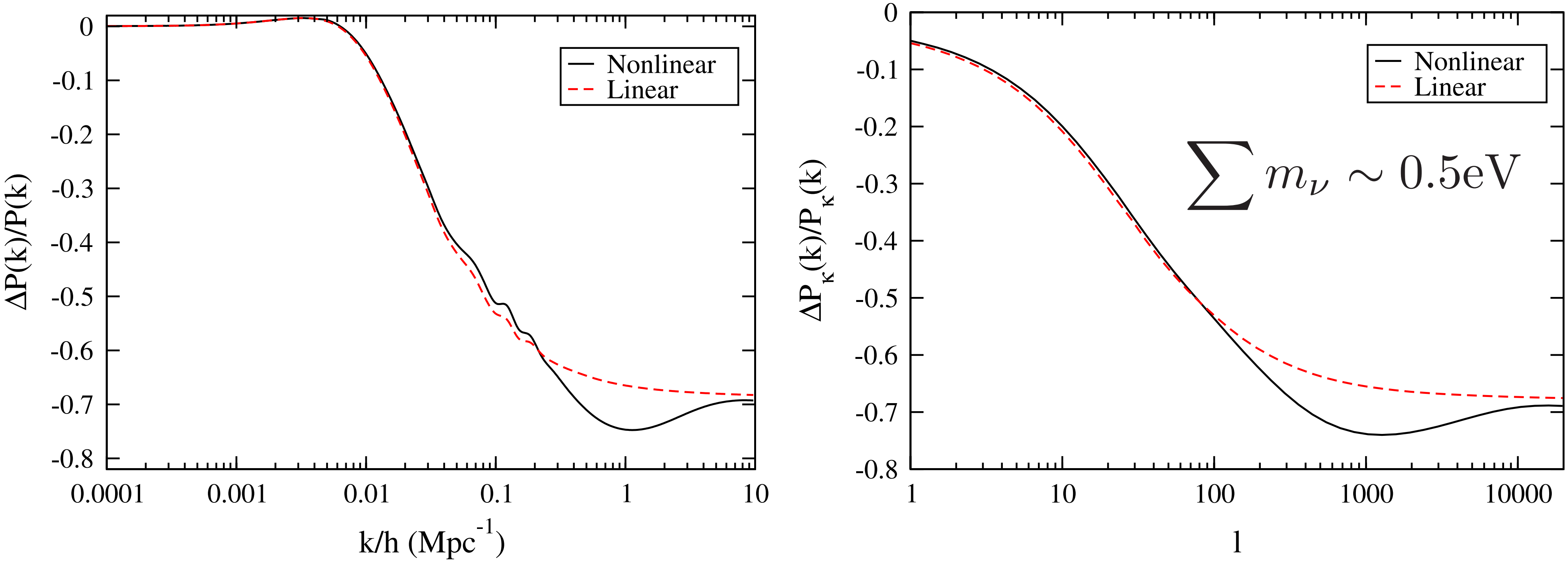


FIG. 1 (color online). *Left panel*: A fractional difference between the matter power spectra for a concordance ΛCDM model ($\Omega_{m0} = 0.3$) and a model with finite-mass neutrinos ($\Omega_{cb0} = 0.27$ and $\Omega_{\nu 0} = 0.03$). Note that the total matter density $\Omega_{m0}(= \Omega_{cb0} + \Omega_{\nu 0})$ and other cosmological parameters are fixed for the two models. The solid curve shows the model prediction including the correction of nonlinear mass clustering (see the text for details), while the dashed curve shows the linear-theory prediction. The finite-mass neutrinos cause a suppression in the power spectrum amplitudes on scales below the free-streaming scale. The suppression effect is enhanced over transition scales between linear and nonlinear regimes. *Right panel*: A similar plot, but for the lensing power spectrum as a function of multipoles $l$.

# Matter power spectrumへのニュートリノの影響

Ichiki et al 2009

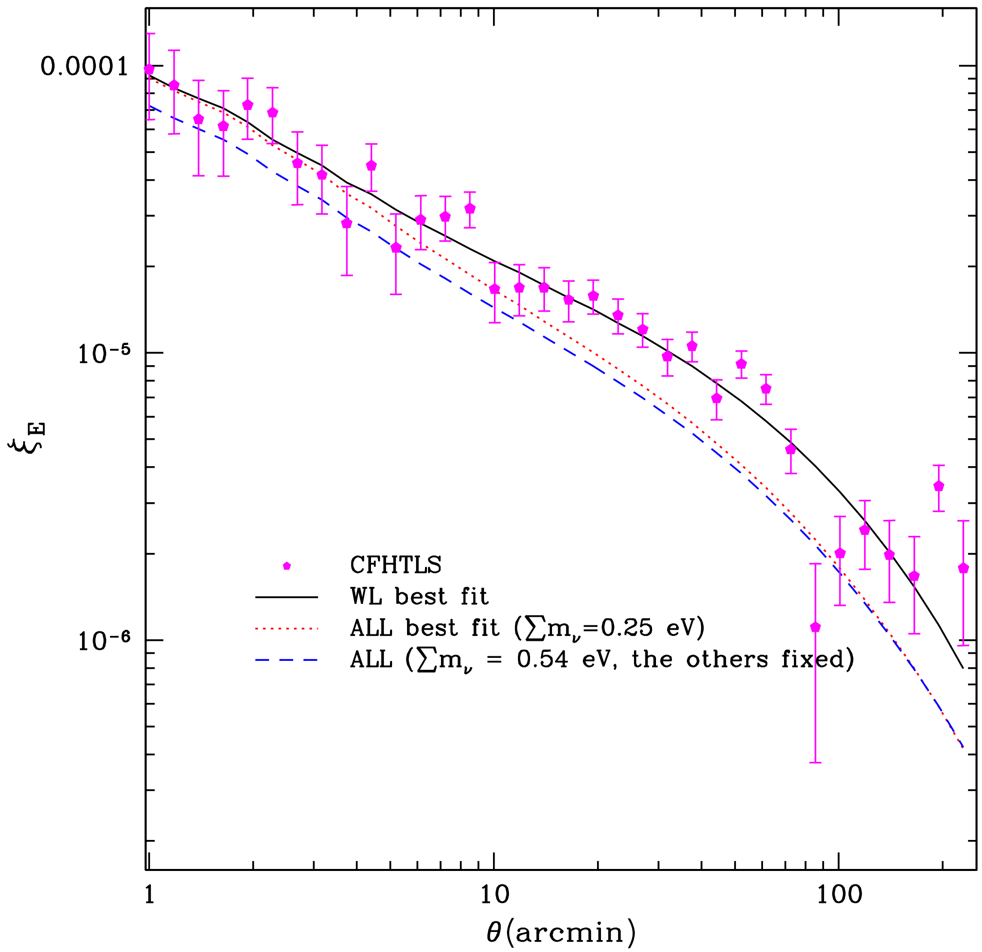


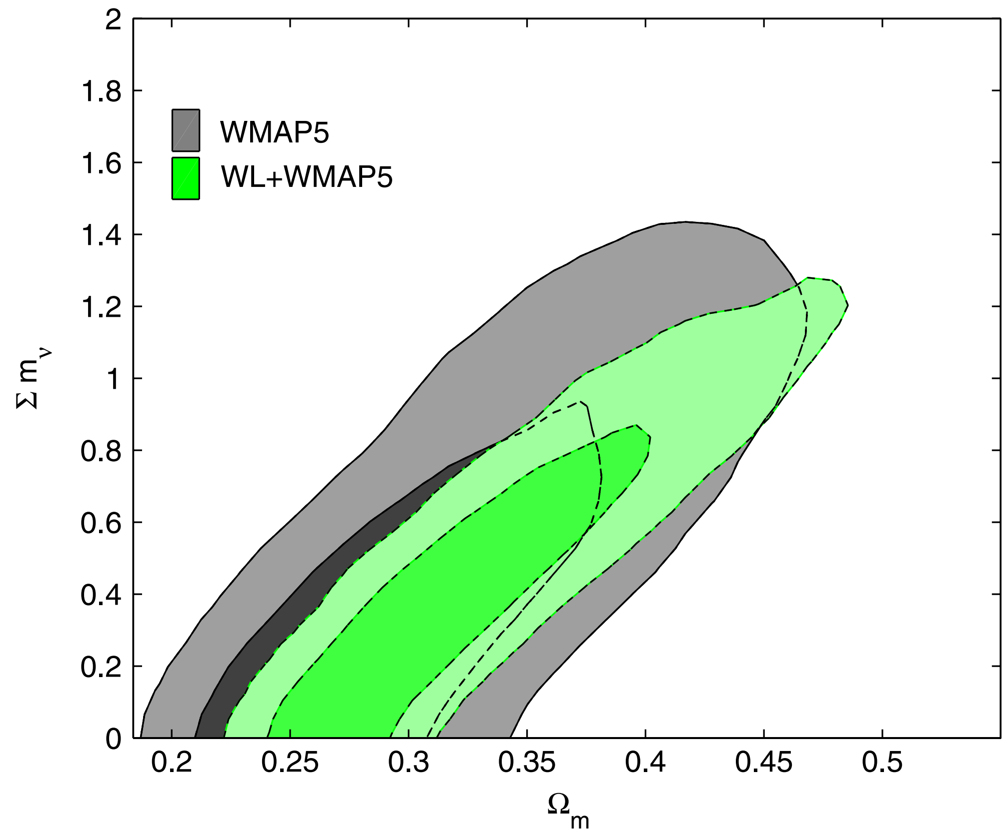

# 最近の結果ーCFHTLenS

- Heymans et al 2013
- 154 deg$^2$
- ng=11/arcmin$^2$
- shape measurement = Lensfit (model fitting)
- 6 redshift bins
- intrinsic alignment - 1 parameter model
- covariance matrix from numerical simulation

$$P_{\mathrm{II}}(k,z) = F^2(z) P_\delta(k,z)$$

$$P_{\mathrm{GI}}(k,z) = F(z) P_\delta(k,z)\,,$$

$$F(z) = -A C_1 \rho_{\mathrm{crit}} \frac{\Omega_{\mathrm{m}}}{D(z)}\,.$$

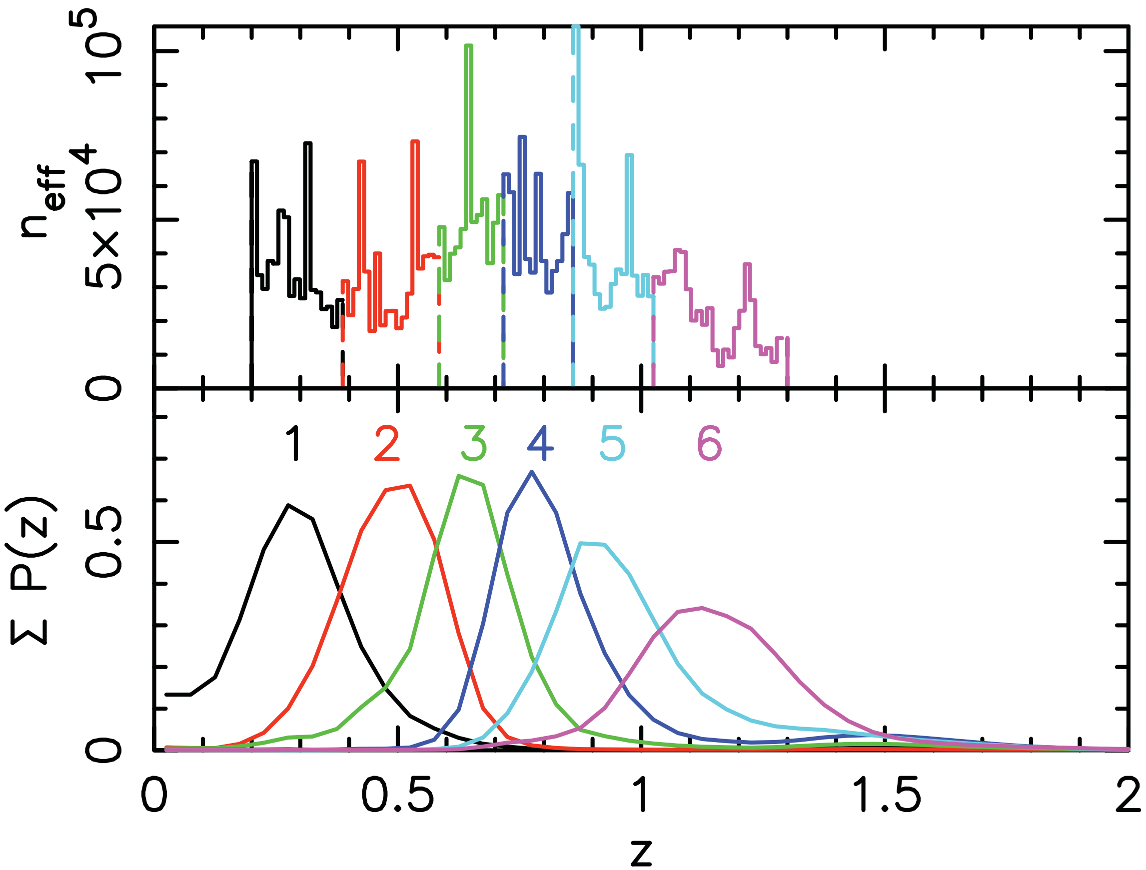

# 最近の結果ーCFHTLenS

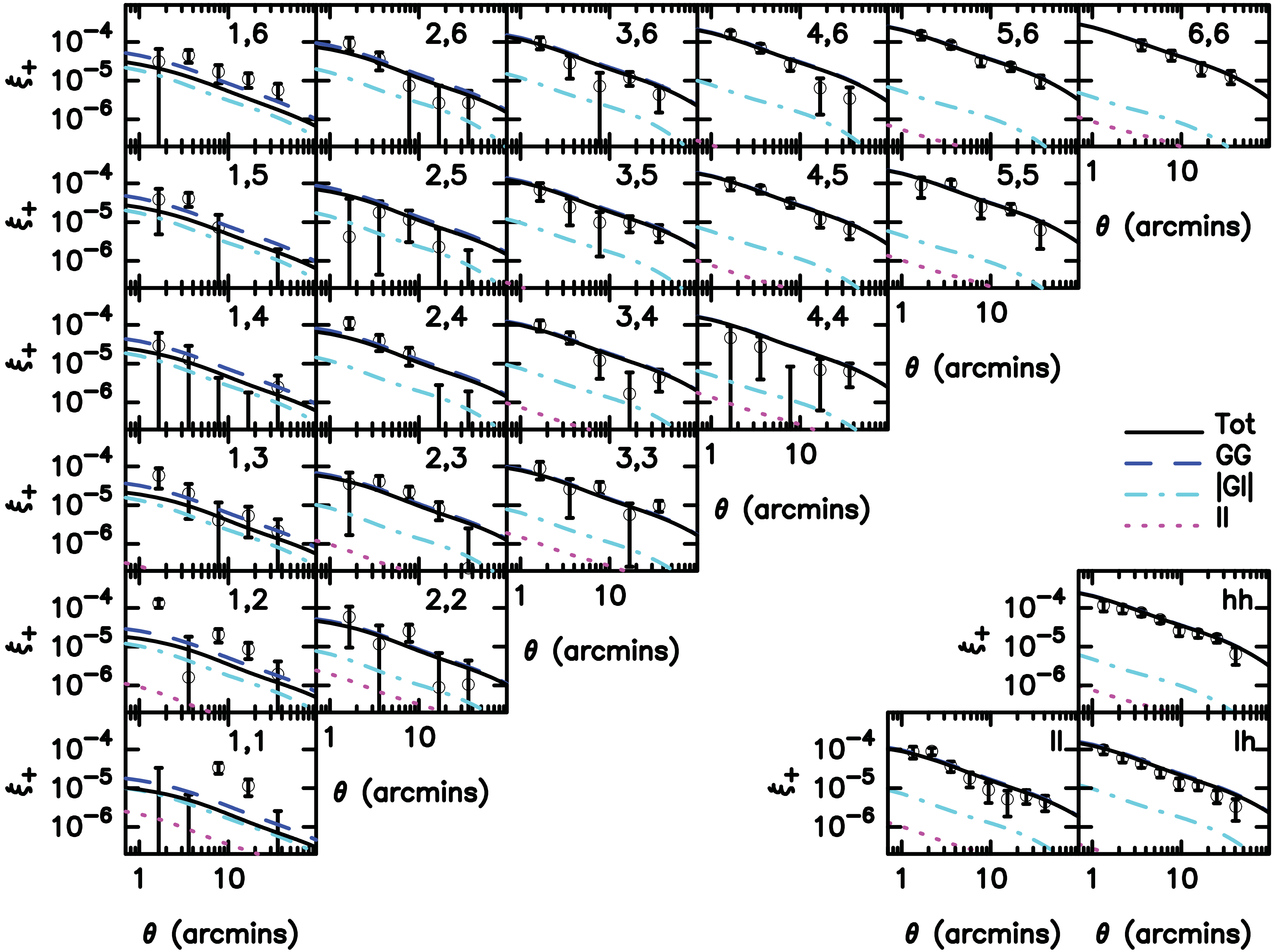

# 最近の結果ーCFHTLenS

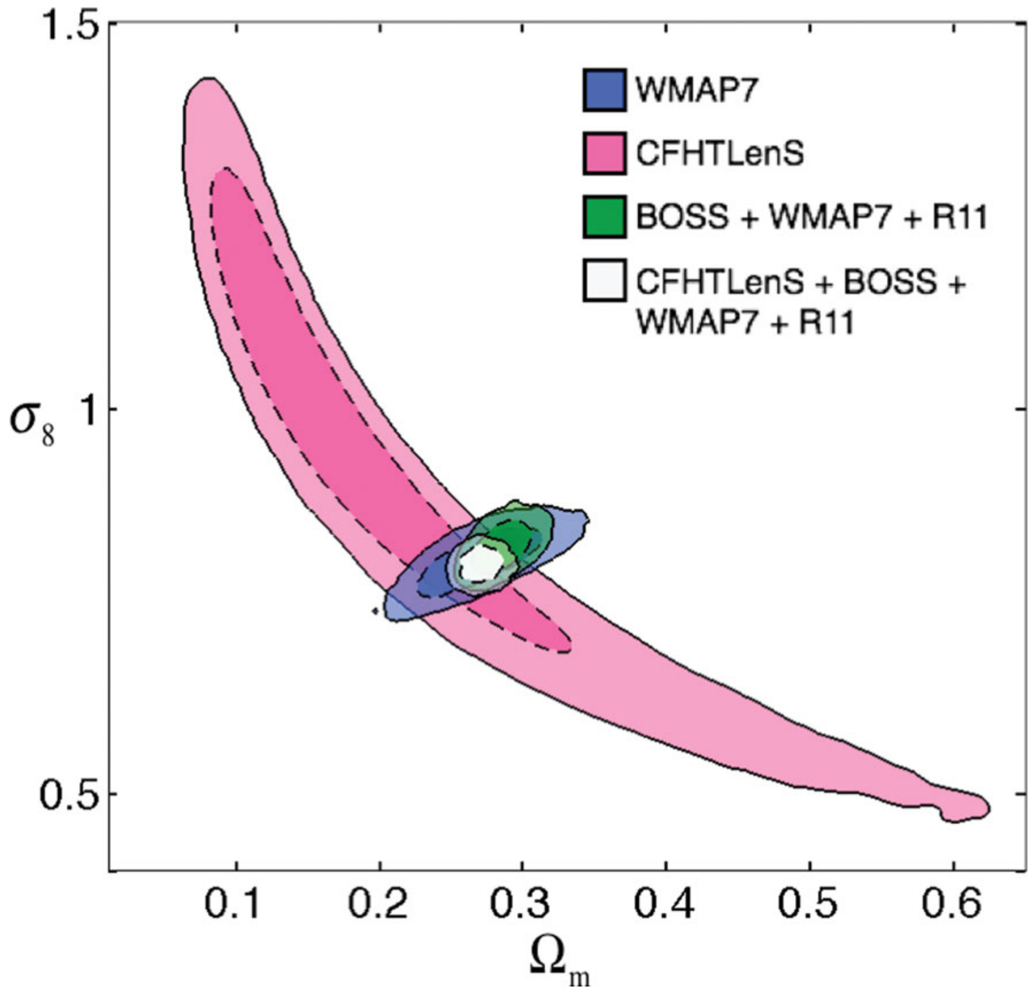


**Figure 5.** Flat ΛCDM joint parameter constraints (68 and 95 per cent confidence) on the amplitude of the matter power spectrum controlled by $\sigma_8$ and the matter density parameter $\Omega_{\mathrm{m}}$ from CFHTLenS-only (pink), *WMAP*7-only (blue), BOSS combined with *WMAP*7 and R11 (green), and CFHTLenS combined with BOSS, *WMAP*7 and R11 (white).

# 最近の結果ーCFHTLenS

$$A_{\rm late} = 0.18^{+0.83}_{-0.82}\,, \quad \leftarrow 80\%$$

$$A_{\rm early} = 5.15^{+1.74}_{-2.32}\,,$$

$$A^{\rm opt}_{\rm early} = 4.26^{+1.23}_{-1.39}\,, \quad \leftarrow 20\%$$

$$A_{\rm all} = -0.48^{+0.75}_{-0.87}\,.$$

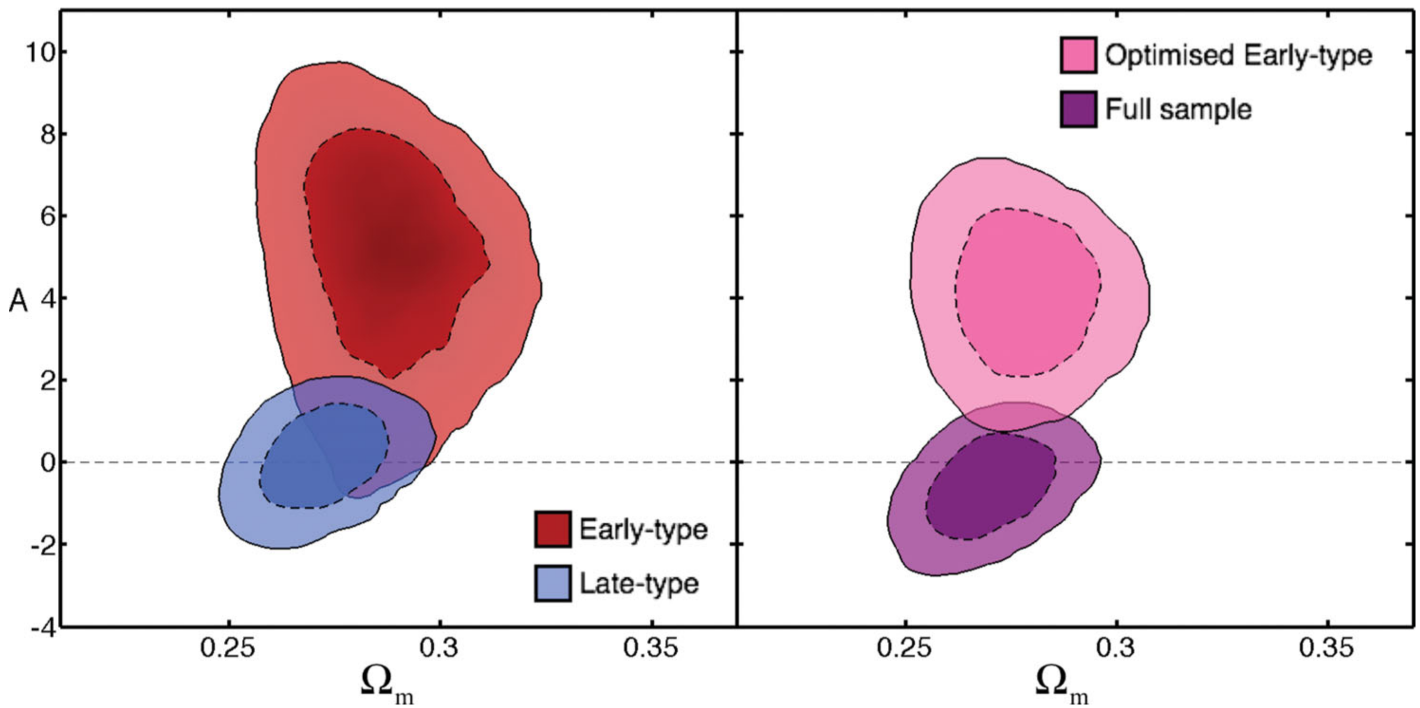


**Figure 11.** Joint parameter constraints on the amplitude of the intrinsic alignment model $A$ and the matter density parameter $\Omega_{\rm m}$ from CFHTLenS combined with *WMAP*7, BOSS and R11. In the left-hand panel, the constraints can be compared between two-galaxy samples split by SED type, (early type in red and late type in blue). In the right-hand panel, we present constraints from an optimized analysis to enhance the measurement of the intrinsic alignment amplitude of early-type galaxies (pink). The full sample, combining early and late-type galaxies, produces an intrinsic alignment signal that is consistent with zero (shown purple). A flat $\Lambda$CDM cosmology is assumed.

# 最近の結果ーDES science verification data

- Becker et al 2016 & Abbott et al 2016
- 139 deg$^2$
- ng=6(4)/arcmin$^2$ for ngmix(im3shape)
- shape = ngmix & im3shape (model fitting)
- 3 redshift bins
- intrinsic alignment - 1 or 2 parameter model
- covariance matrix from Jackknife & Num. sim.

$$F(z, \eta_{\rm other}) = -A C_1 \rho_{\rm crit} \frac{\Omega_{\rm m}}{D(z)} \left( \frac{1+z}{1+z_0} \right)^{\eta_{\rm other}} .$$

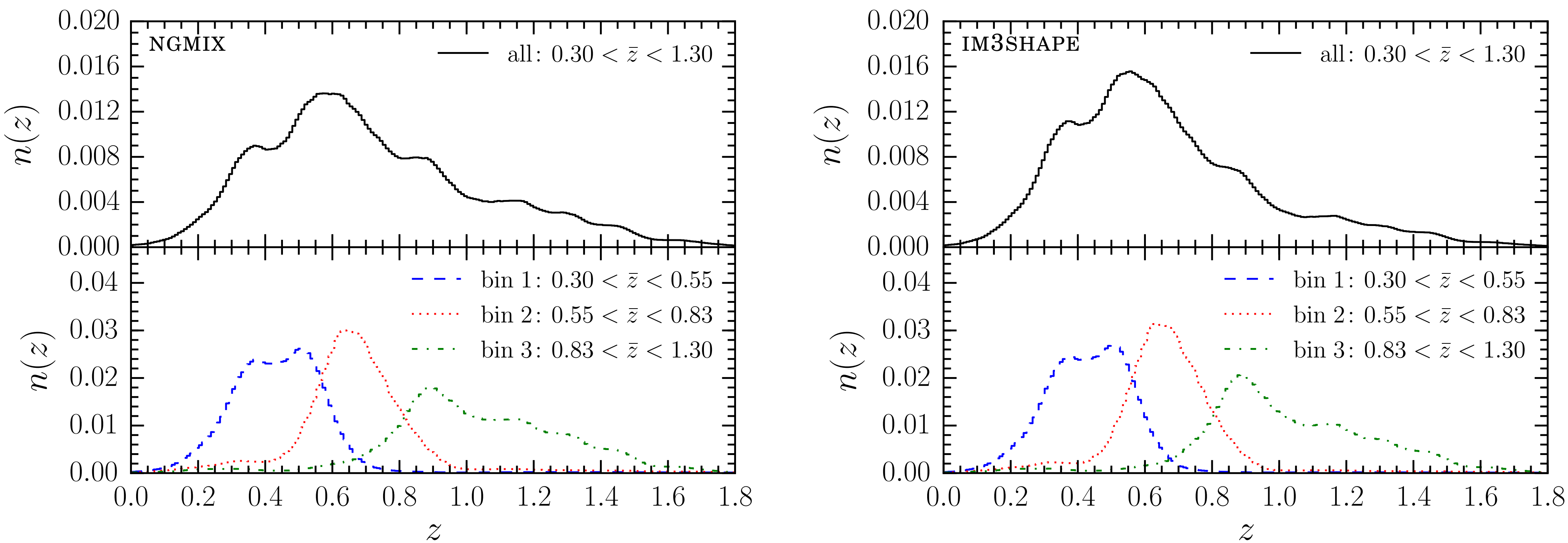

# 最近の結果ーDES science verification data

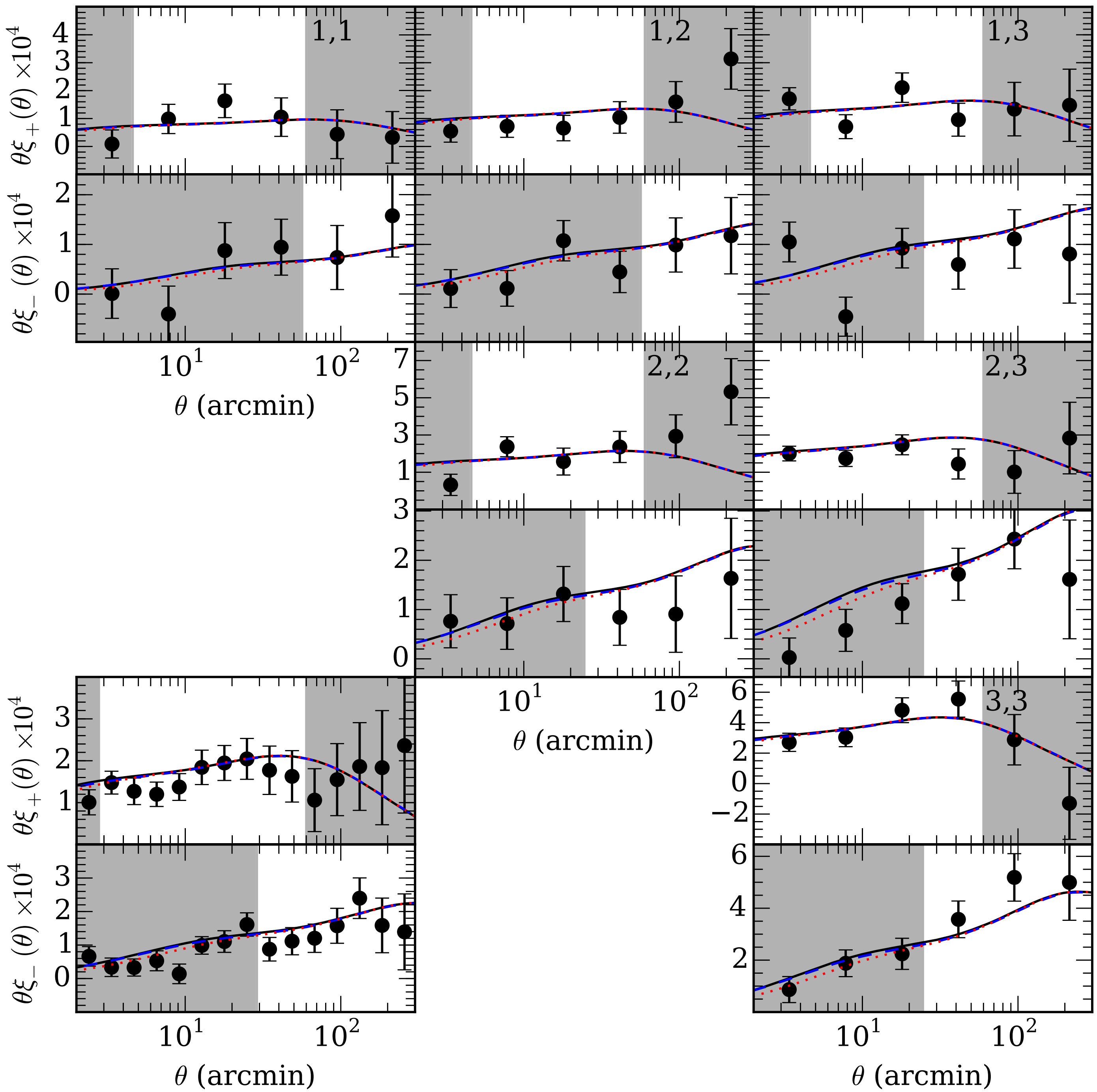

# 最近の結果ーDES science verification data

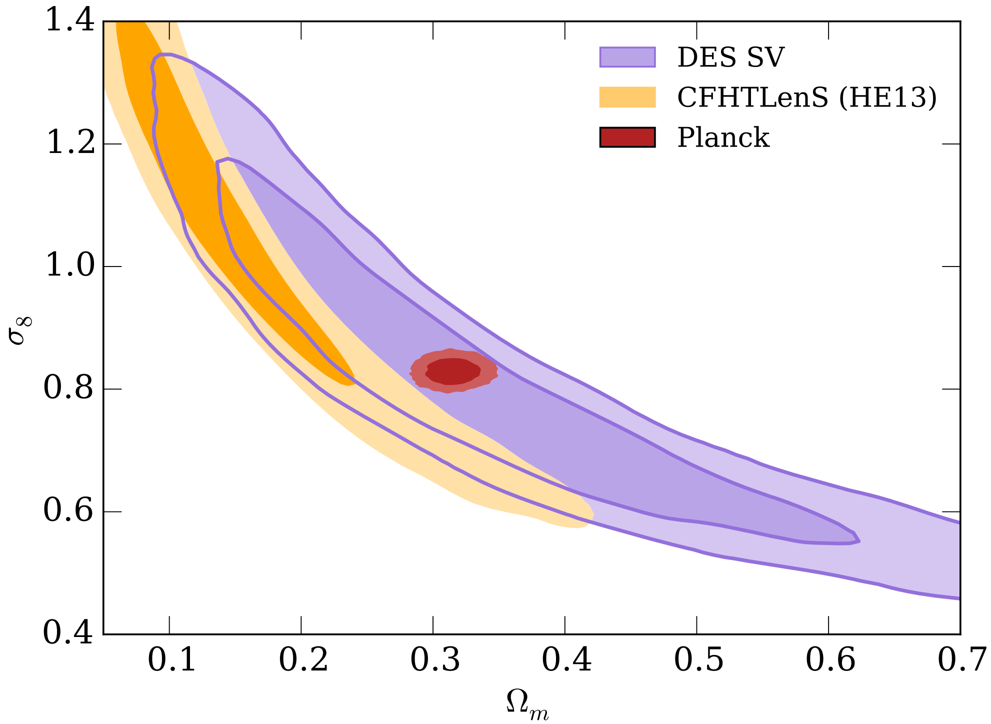


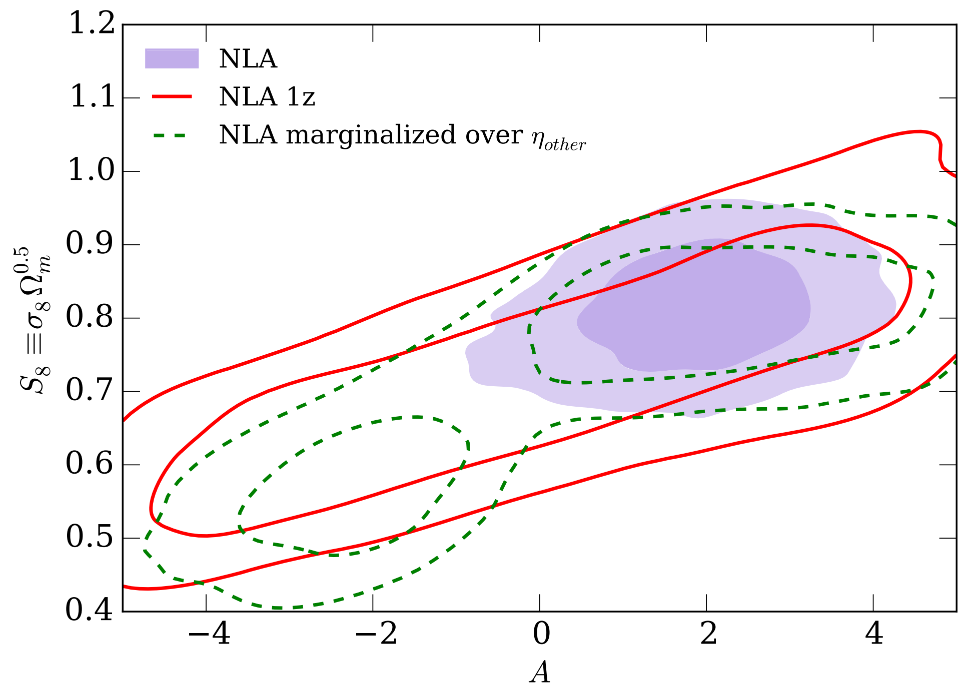

# 最近の結果ーKidS-450

- Hildebrandt et al 2016
- 450 deg$^2$
- ng=8/arcmin$^2$
- shape measurement = Lensfit (model fitting)
- 4 redshift bins
- intrinsic alignment - 3 parameter model
- Baryon effect model - 1 parameter (Mead )
- covariance matrix from Jackknife & Num. sim.

$$F(z) = -A_{\rm IA} C_1 \rho_{\rm crit} \frac{\Omega_{\rm m}}{D_+(z)} \left(\frac{1+z}{1+z_0}\right)^{\eta} \left(\frac{\bar{L}}{L_0}\right)^{\beta} . \qquad (8)$$

# 最近の結果ーKidS-450

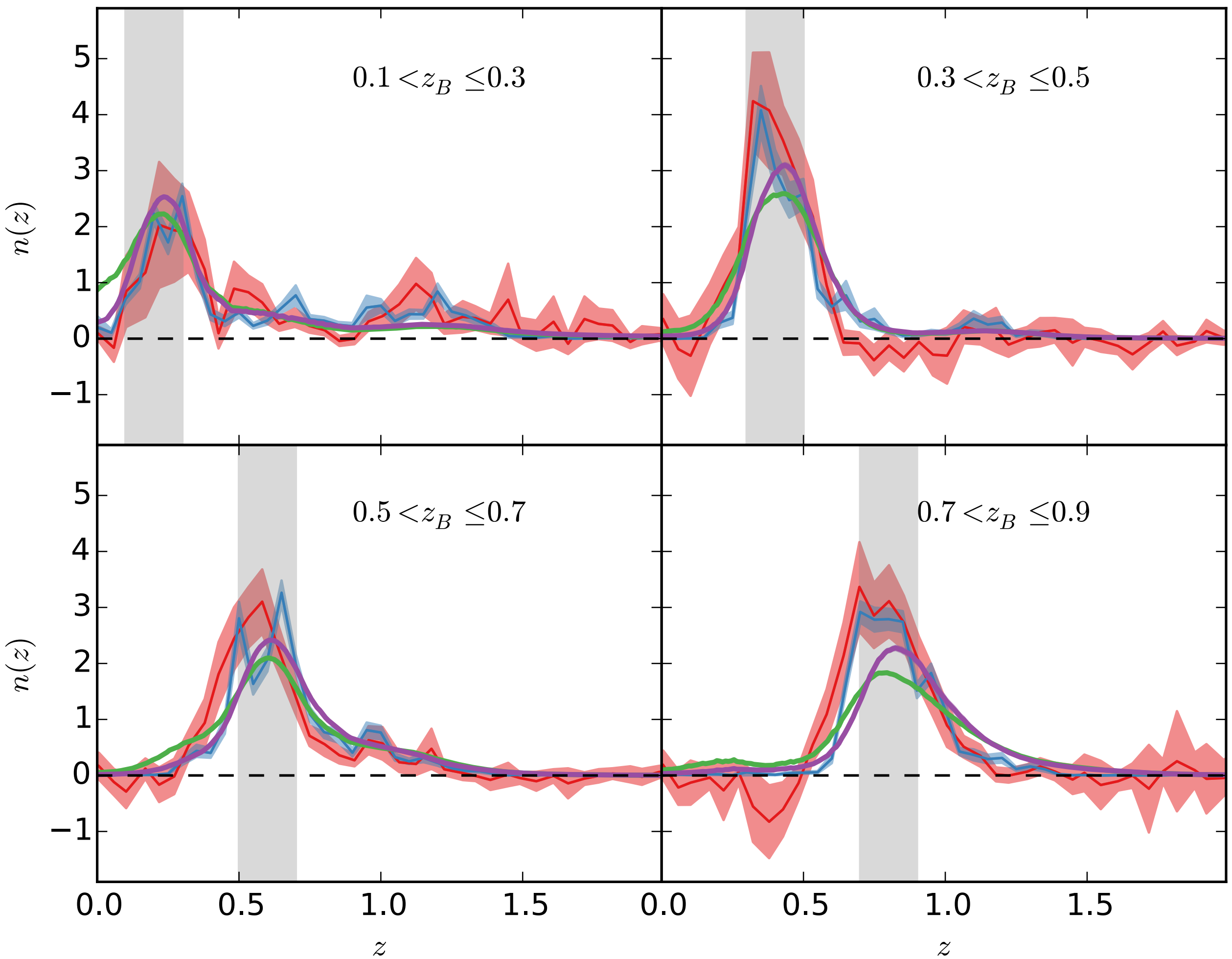


**Figure 2.** Comparison of the normalised redshift distributions for the four tomographic bins as estimated from the weighted direct calibration (DIR, blue with errors), the calibration with cross-correlations (CC, red with errors), the re-calibrated stacked $P_{\rm recal}(z)$ (BOR, purple with errors that are barely visible), and the original stacked $P(z)$ from BPZ (green). The gray-shaded regions indicate the target redshift range selected by cuts on the Bayesian photo-$z$ $z_{\rm B}$.

# 最近の結果ーKidS-450

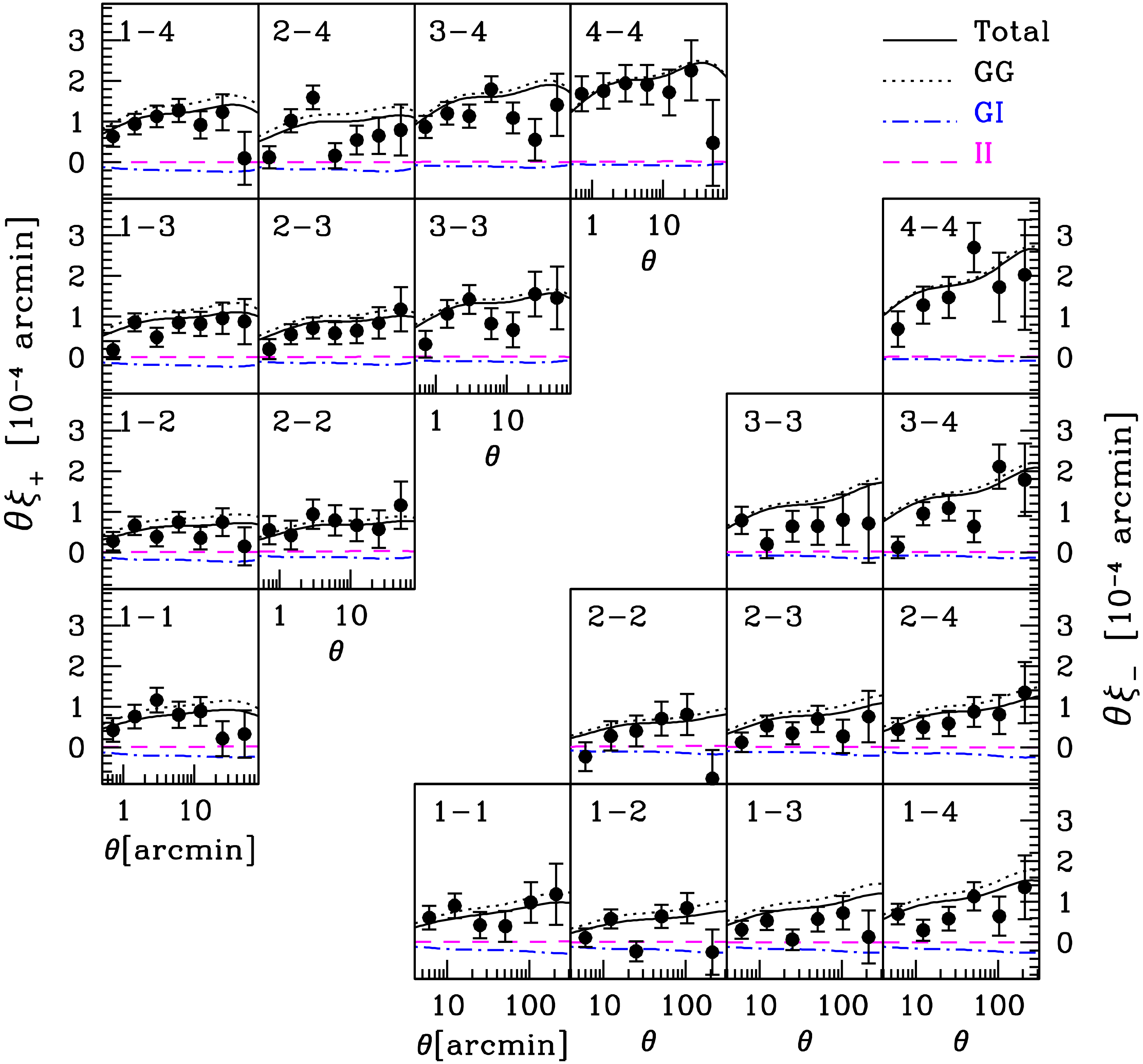

# 最近の結果ーKidS-450

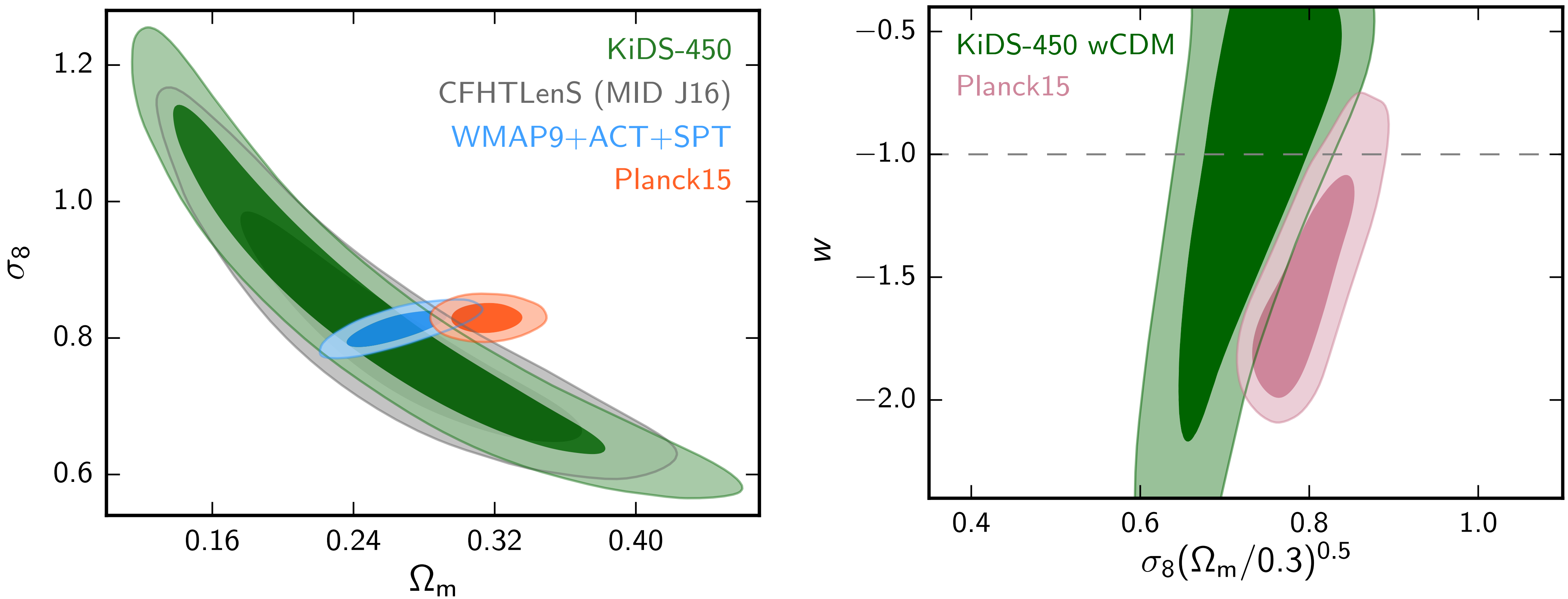

# 最近の結果ーKidS-450

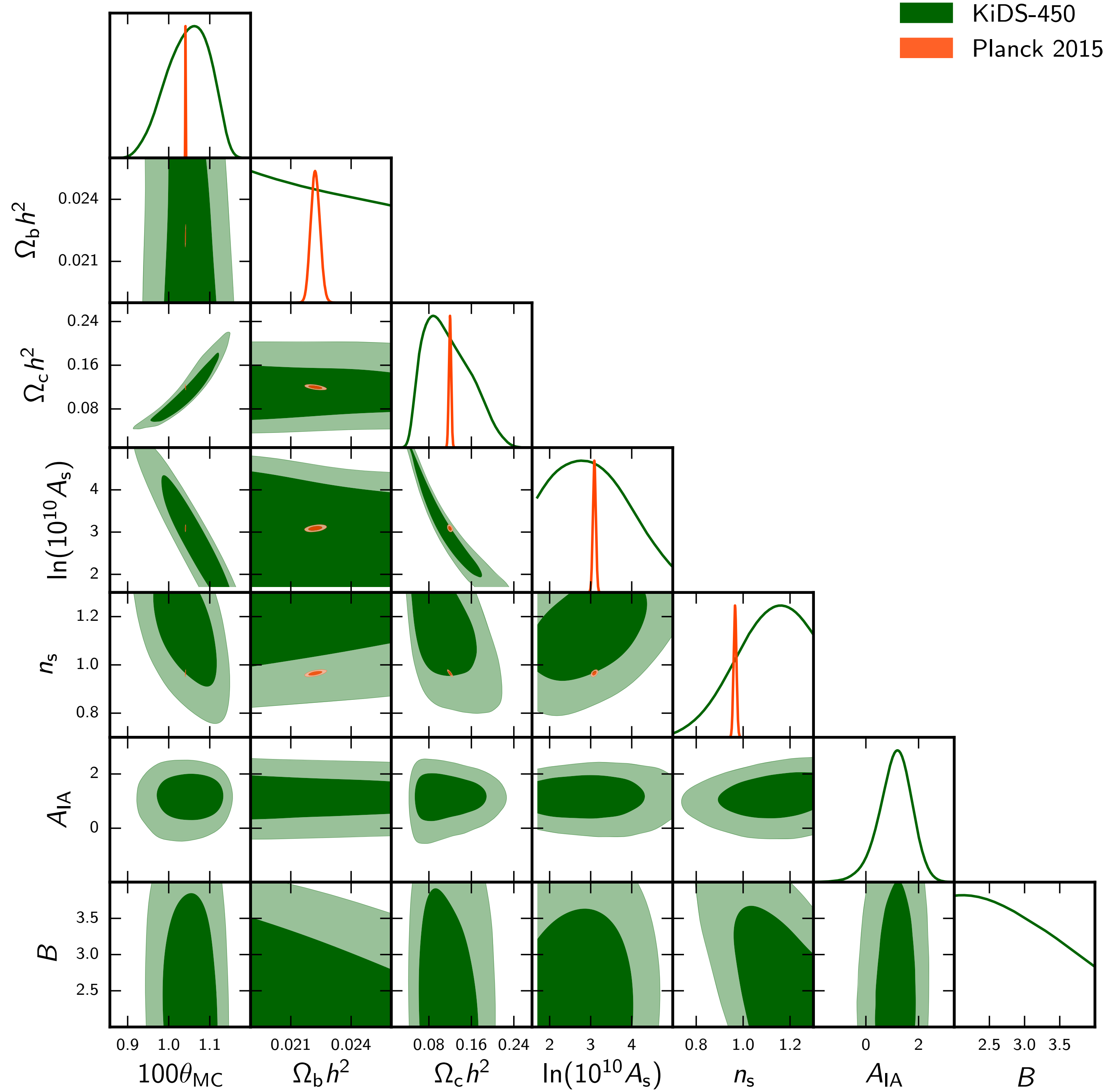

# 最近の結果ーHSC survey

- S16A wide --- 170 $deg^2$
- ng=16(22)/$arcmin^2$ for $i<24.5$($i<25$)
- shape = HSM_regauss (Hirata & Seljak 2003, Mandelbaum et al 2005 )
  - shape measurementのcalibrationは現在進行中
  - 結果はshape catalog 論文にて公表
- 5 photo-z available (明日の田中さんの講義)
- データアクセスは明日の実習

# HSC catalogでのlensing shape情報

•"ixxx" = i-band imageより計測された

•"shape_hsm_regauss" = Hirata, Seljak, Mandelbaumによって開発された regauss法で計測された量

- •ishape_hsm_regauss_e1 = PSF補正後の"$e_1$"
- •ishape_hsm_regauss_e2 = PSF補正後の"$e_2$"
- •ishape_hsm_regauss_sigma = eの統計誤差／各成分
- •ishape_hsm_regauss_resolution = 銀河のサイズを表すパラメーター

  1-trace(Q_PSF)/trace(Q_object)

•"shape_sdss" = SDSSで用いられていたadopted momentで定義された量

- •`ishape_sdss_i11 = sdss adopted moment`の11成分
- •`ishape_sdss_psf_i11 = object`の位置での`PSF`の`sdss adopted moment`の11成分

# HSC catalogでのlensing shape情報

注１）shapeの”e”はsky座標（RA,Dec）で定義されているので
object間の離角や、eを(tangent,cross)成分へ変換するさいの角度は球面３角法を用いる

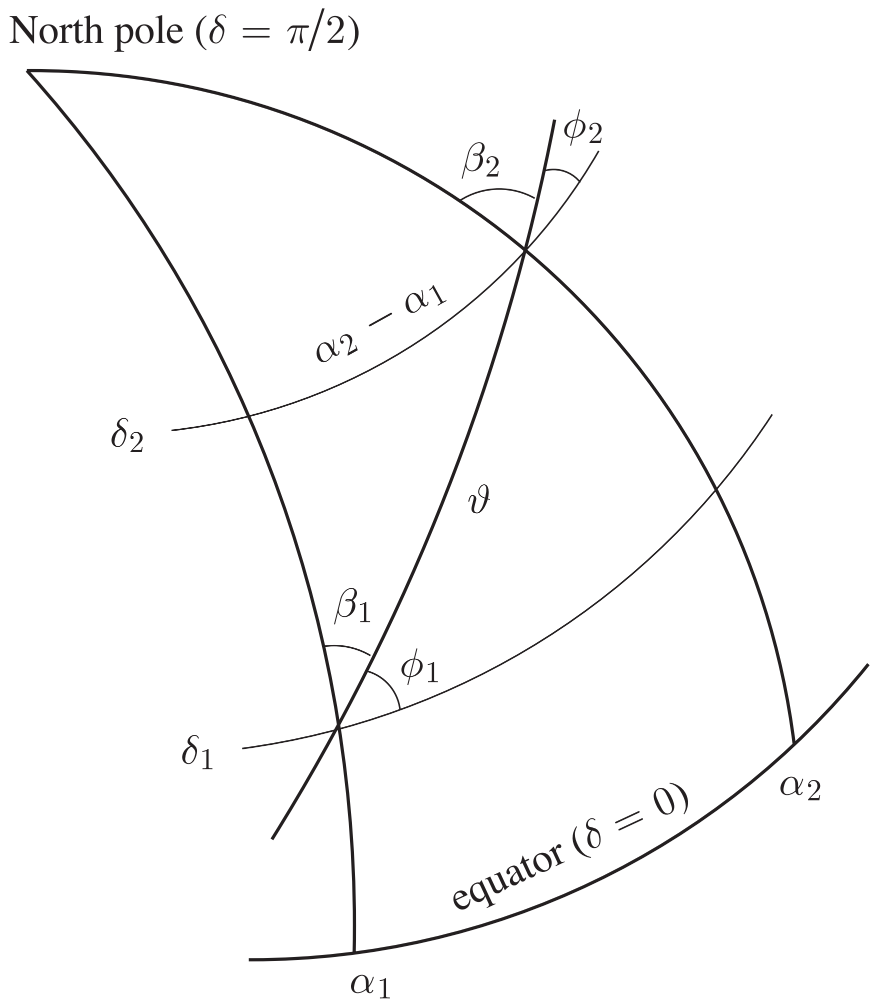


**Figure 2.** Angles and coordinates on a sphere for two galaxies $i = 1, 2$ located at ($\alpha_i$, $\delta_i$). Great circle segments are drawn as bold lines.

＊Kilbinger et al (2013)のspherical trigonometryの解説での座標系の定義はHealpixとは違います。

# HSC catalogでのlensing shape情報

注２）hsm_regaussの場合のweightはinverse variance weightを採用して

$$
\begin{aligned}
w &= \frac{1}{\sigma_e^2 + e_{stat}^2} \\
&= \frac{1}{0.365^2 + \mathrm{ishape\_hsm\_regauss\_sigma}^2}
\end{aligned}
$$

注３）$e \to g \sim \gamma$

$$\tilde{\gamma}_1 = \frac{\mathrm{ishape\_hsm\_regauss\_e1}}{2(1-\sigma_e^2)} \simeq \frac{\mathrm{ishape\_hsm\_regauss\_e1}}{2(1-0.365^2)}$$

$$\tilde{\gamma}_2 = \frac{\mathrm{ishape\_hsm\_regauss\_e2}}{2(1-\sigma_e^2)} \simeq \frac{\mathrm{ishape\_hsm\_regauss\_e2}}{2(1-0.365^2)}$$

# HSC catalogでのlensing shape情報

注４）HSC weak lensing working groupで推奨されている選択条件

```
icmodel_flux/icmodel_flux_err > 10

ishape_hsm_regauss_resolution > 0.3

ishape_hsm_regauss_e1^2 +ishape_hsm_regauss_e2^2 < 4

ishape_hsm_regauss_sigma < 0.4

icmodel_mag < 24.5
```